CHAPTER 17
PULSE DOPPLER RADAR

William H. Long
David H. Mooney
William A. Skillman
Westinghouse Electric Corporation

17.1 CHARACTERISTICS AND APPLICATIONS

Nomenclature. For the purpose of this chapter, the term *pulse doppler* (PD) will be used for radars to which the following apply:

1. They utilize coherent transmission and reception; that is, each transmitted pulse and the receiver local oscillator are synchronized to a free-running, highly stable oscillator.

2. They use a sufficiently high pulse repetition frequency (PRF) to be ambiguous in range.

3. They employ coherent processing to reject main-beam clutter, enhance target detection, and aid in target discrimination or classification.

Applications. PD is applied principally to radar systems requiring the detection of moving targets in a severe clutter environment. Table 17.1 lists typical applications [1-10] and requirements. This chapter will deal principally with airborne applications, although the basic principles can also be applied to the ground-based case.

PRFs. Pulse doppler radars are generally divided into two broad PRF categories: medium and high PRF.[11] In a medium-PRF radar[12-14] the target and clutter ranges and velocities of interest are usually ambiguous, while in a high-PRF radar [15] the range is ambiguous but the velocity is unambiguous (or has at most a single velocity ambiguity as discussed later).

A low-PRF radar, commonly called a moving-target indicator (MTI),[16] is one in which the ranges of interest are unambiguous while the velocities are usually ambiguous. MTI radars are generally not categorized as pulse doppler radars, although the principles of operation are similar. A comparison of MTI and pulse doppler radars is shown in Table 17.2.

TABLE 17.1   Pulse Doppler Applications and Requirements

Radar application	Requirements
Airborne or spaceborne surveillance	Long detection range; accurate range data
Airborne interceptor or fire control	Medium detection range; accurate range, velocity data
Ground-based surveillance	Medium detection range; accurate range data
Battlefield surveillance (slow-moving target detection)	Medium detection range; accurate range, velocity data
Missile seeker	May not need true range information
Ground-based weapon control	Short range; accurate range, velocity data
Meteorological	High velocity and range data resolution
Missile warning	Short detection range; very low false-alarm rate

TABLE 17.2   Comparison of MTI and Pulse Doppler (PD) Radars

	Advantages	Disadvantages
MTI—low PRF	Can sort clutter from targets on basis of range. No range ghosts. Front-end STC suppresses sidelobe detections and reduces dynamic range requirements.	Low doppler visibility due to multiple blind speeds. Poor slow-moving target rejection. Cannot measure radial target velocity.
PD—medium PRF	Good performance at all target aspects. Good slow-moving target rejection. Measures radial velocity. Less range eclipsing than in high PRF.	Range ghosts. Sidelobe clutter limits performance. High stability requirements due to range folding.
PD—high PRF	Can be sidelobe clutter–free for some target aspects. Single doppler blind zone at zero velocity. Good slow-moving target rejection. Measures radial velocity. Velocity-only detection can improve detection range.	Sidelobe clutter limits performance. Range eclipsing. Range ghosts. High stability requirements due to range folding.

Pulse Doppler Spectrum.   The transmitted spectrum of a pulse doppler radar consists of discrete lines at the carrier frequency f_0 and at sideband frequencies $f_0 \pm i f_R$, where f_R is the PRF and i is an integer. The envelope of the spectrum is determined by the pulse shape. For the rectangular pulses usually employed, a $(\sin x)/x$ spectrum is obtained.

The received spectrum from a stationary target has lines that are doppler-shifted proportionally to the line of sight, or radial velocity, between the radar platform and the target. The two-way doppler shift is given by $f_d = (2V_R/\lambda) \cos \psi_0$, where λ is the radar wavelength, V_R is the radar platform velocity, and ψ_0 is
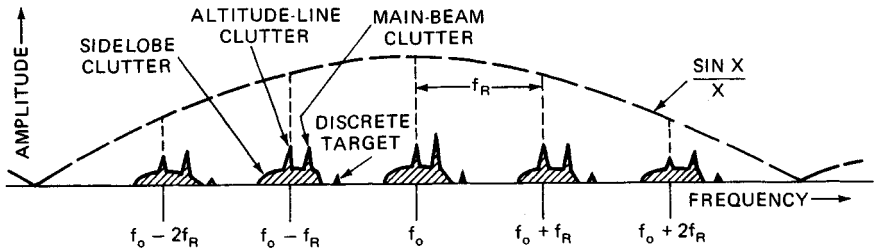
FIG. 17.1 Clutter and target frequency spectrum from a horizontally moving platform.

the angle between the velocity vector and the line of sight to the target. Illustrated in Fig. 17.1 is the received pulsed spectrum with returns from continuous clutter, such as the ground or clouds, and from discrete targets, such as aircraft, automobiles, tanks, etc.

Figure 17.2 shows the unfolded spectrum (i.e., no spectral foldover from adjacent PRF lines) in the case of horizontal motion of the radar platform, with a velocity V_R. The clutter-free region is defined as that portion of the spectrum in which no ground clutter can exist. (A clutter-free region usually does not exist with medium PRFs.) The sidelobe clutter region, $4V_R/\lambda$ in width, contains ground clutter power from the sidelobes of the antenna, although the clutter power may be below the noise level in part of the region. The main-beam region, located at $f_0 + (2V_R/\lambda)$ cos ψ_0, contains the strong return from the main beam of the antenna striking the ground at a scan angle of ψ_0, measured from the velocity vector. Rain and chaff clutter may also be large when the main beam illuminates a rain or chaff cloud. Motion due to winds may displace and/or spread the return in frequency.

Altitude-line clutter, which is due to ground clutter at near normal incidence directly below the radar platform, is at zero doppler if there is no vertical component of platform velocity. A discrete target return in the main beam is shown at $f_T = f_0 + (2V_R/\lambda)$ cos $\psi_0 + (2V_T/\lambda)$ cos ψ_T, where the target velocity is V_T, with an angle ψ_T between the target velocity vector and the radar target line of sight.
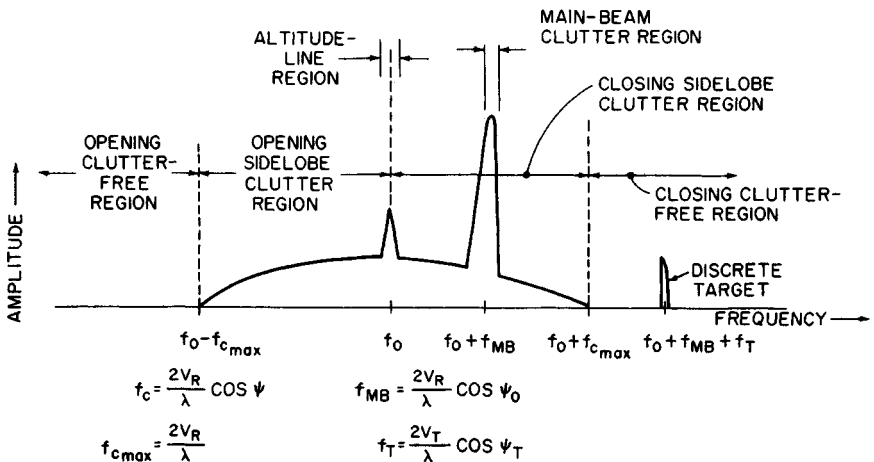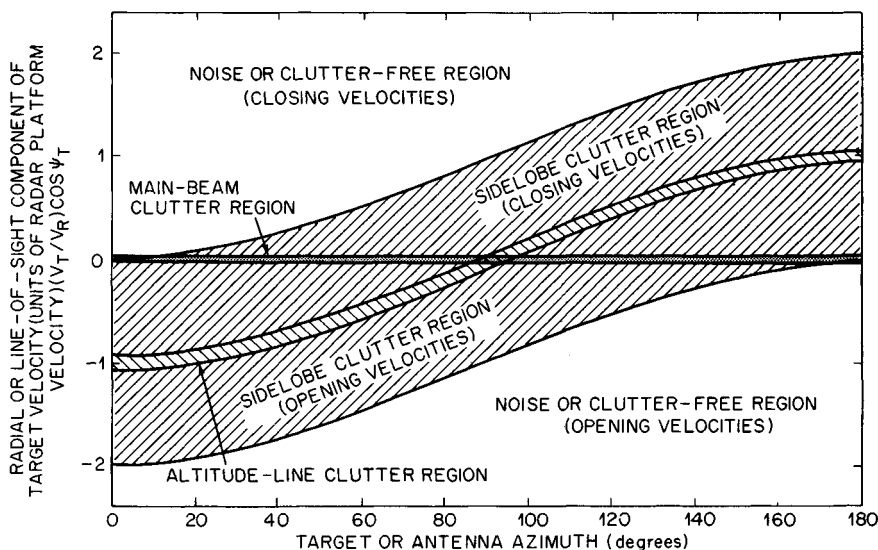

FIG. 17.2 Unfolded spectrum (with no clutter tracking).

The components of the spectrum shown in Fig. 17.2 will also vary with range as discussed later.

Figure 17.3 illustrates the various clutter doppler frequency regions as a function of the antenna azimuth and relative radar and target velocities, again for an unfolded spectrum. The ordinate is the radial, or line-of-sight, component of target velocity in units of radar platform velocity, so that the main-beam clutter region is at zero velocity and the sidelobe clutter region frequency boundaries vary sinusoidally with antenna azimuth. Thus, it shows the doppler regions in which the target can become clear of sidelobe clutter. For example, if the antenna azimuth angle is at zero, any head-on target ($V_T \cos \psi_T > 0$) is clear of sidelobe clutter, whereas if the radar is in trail behind the target ($\psi_T = 180°$ and $\psi_0 = 0°$), the target's radial velocity has to be greater than twice that of the radar to become clear of sidelobe clutter.

The sidelobe clear and clutter regions can also be expressed in terms of the aspect angle with respect to the target,[14] as shown in Fig. 17.4. Here, collision geometry is assumed in which the radar and target aircraft fly straight-line paths toward an intercept point; the look angle of the radar ψ_0 and the aspect angle of the target ψ_T are constant for a given set of radar and target speeds V_R and V_T, respectively. The center of the diagram is the target, and the angle to the radar on the circumference is the aspect angle. The aspect angle and look angles satisfy the equation $V_R \sin \psi_0 = V_T \sin \psi_T$, which is defined as a collision course. The target aspect angle is zero for a head-on condition and 180° for a tail chase. The aspect angle corresponding to the boundary between the sidelobe clutter region and the sidelobe clear region is a function of the relative radar-target velocity ratio and is shown in Fig. 17.4 for four cases. Case 1 is where the radar and target speeds are equal and the target can be seen clear of sidelobe clutter in a head-on

FIG. 17.3 Clutter and clutter-free regions as a function of target velocity and azimuth.
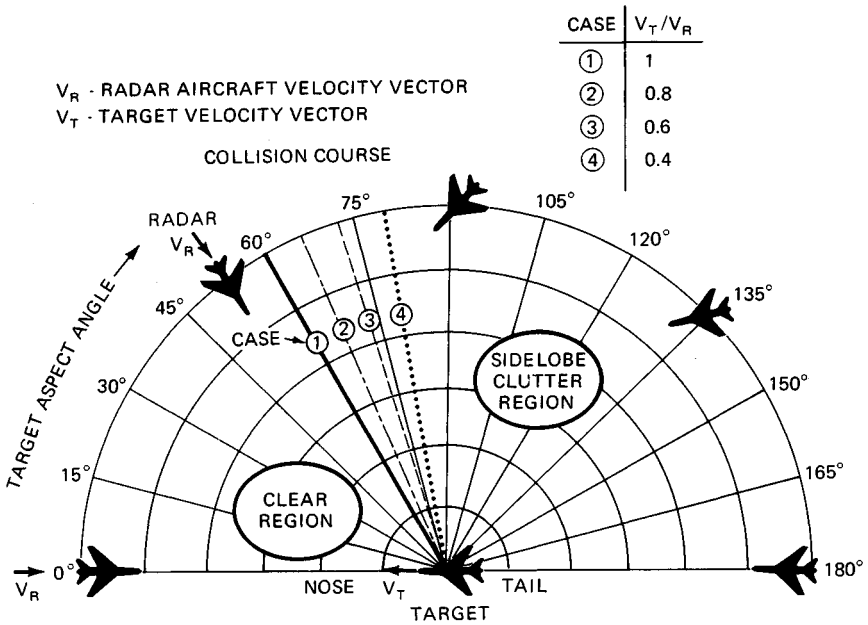
FIG. 17.4   Sidelobe clutter-clear regions versus target aspect angle.

aspect out to 60° on either side of the target's velocity vector. Similarly, Cases 2 to 4 show conditions where the target's speed is 0.8, 0.6, and 0.4 times the radar's speed, in which case the target can be seen clear of sidelobe clutter over a region of up to ±78.5° relative to the target's velocity vector. Again, these conditions are for an assumed collision course. As is evident, the aspect angle of the target clear of sidelobe clutter is always forward of the beam aspect.

Ambiguities and PRF Selection.   Pulse doppler radars are generally ambiguous in either range or doppler, or both. The unambiguous range R_u is given by $c/2f_R$, where c is the speed of light and f_R is the PRF.

If the maximum target velocity to be observed is $\pm V_{T\max}$, then the minimum value of PRF, $f_{R\min}$, which is unambiguous in velocity (both magnitude and doppler sense, i.e., positive and negative), is

$$f_{R\min} = 4V_{T\max}/\lambda \qquad (17.1)$$

However, some pulse doppler radars employ a PRF which is unambiguous in velocity magnitude only, i.e., $f_{R\min} = 2V_{T\max}/\lambda$, and rely on detections in multiple PRFs during the time on target to resolve the ambiguity in doppler sense. These types of radars can be considered to be in the high-PRF category if the older definition of high PRF (no velocity ambiguity) is extended to allow one velocity ambiguity, that of doppler sense. The lower PRF eases the measurement of true range while retaining the high-PRF advantage of a single blind-speed region near zero doppler.

The choice between high and medium PRF involves a number of consider-
ations, such as transmitter duty cycle limit, pulse compression availability,
signal-processing capability, missile illumination requirements, etc., but often de-
pends on the need for all-aspect target detectability. All-aspect coverage requires
good performance in tail chase, where the target doppler is in the sidelobe clutter
region near the altitude line. In a high-PRF radar, the range foldover may leave
little clear region in the range dimension, thus degrading target detectability. By
using a lower or medium PRF, the clear region in range is increased at the ex-
pense of velocity foldover for high-doppler targets that are in the clutter-free re-
gion in high PRF. For example, Fig. 17.5 shows the clutter-plus-noise-to-noise
ratio in range doppler coordinates for a 12-kHz PRF at an altitude of 6000 ft
showing the main-beam clutter, altitude line, and sidelobe clutter. The range di-
mension represents the unambiguous range interval R_u, and the frequency dimen-
sion represents the PRF interval. As is evident, there is a range doppler region in
which the sidelobe clutter is below thermal noise and in which good target
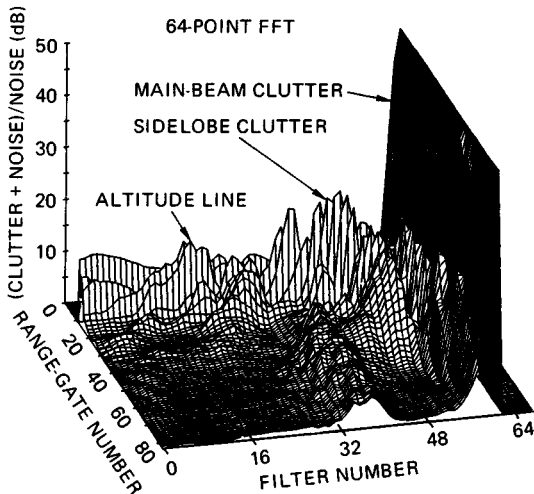detectability can be achieved. The main-beam clutter is filtered out.

FIG. 17.5   Clutter-plus-noise-to-noise ratio in range doppler
space.

Because the clutter is folded in both range and doppler with medium PRF, a
number of PRFs may be required to obtain a satisfactory probability of sufficient
detections to resolve the range and doppler ambiguities. The multiple PRFs move
the relative location of the clear regions so that all-aspect target coverage is
achieved. Since the sidelobe clutter generally covers the doppler region of inter-
est, the ratio of the region with sidelobe clutter below noise relative to the total
range-doppler space is a function of the radar altitude, speed, and antenna
sidelobe level.

If a high-PRF waveform is used, the clear-range region disappears because the
sidelobe clutter folds in range into the unambiguous range interval (assuming the
target doppler is such that it still competes with the sidelobe clutter). However, in

those doppler regions free of sidelobe clutter, as shown in Figs. 17.3 and 17.4, target detectability is limited only by thermal noise, independently of radar altitude, speed, and sidelobe level. This requires system stability sidebands to be well below noise for the worst-case main-beam clutter. Thus, although medium PRF provides all-aspect target coverage, the target is potentially competing with sidelobe clutter at all aspects, whereas with high PRF a target can become clear of sidelobe clutter at aspect angles forward of the beam aspect.

Basic Configuration. Figure 17.6 shows a representative configuration of a pulse doppler radar utilizing digital signal processing under the control of a central computer. Included are the transmitter suppression circuits, main-beam and sidelobe discrete rejection circuits, and ambiguity resolvers. The radar computer receives inputs from the on-board systems, such as the inertial unit and operator controls, and performs as a master controller for the radar. As such, it does the track loop and automatic gain control (AGC) loop filtering, antenna scan pattern generation, and clutter positioning as well as the target-processing functions (such as centroiding). In addition, the computer performs the multiple-target track functions when the radar is in a track-while-scan mode and may execute radar self-test and calibration routines. For simplicity only the search processing is shown.

Duplexer. The duplexer in a pulse doppler radar is usually a passive device such as a circulator which effectively switches the antenna between the transmitter and receiver. Considerable power may be coupled to the receiver since typically 20 to 25 dB isolation may be expected from ferrite circulators.

Receiver-Protector (R/P). The receiver-protector is a fast-response, high-power switch which prevents the transmitter output from the duplexer from damaging the sensitive receiver front end. Fast recovery is required to minimize desensitization in the range gates following the transmitted pulse.

RF Attenuator. The RF attenuator is used both for suppressing transmitter leakage from the R/P into the receiver (so that the receiver is not driven into saturation, which could lengthen recovery time after the transmitter is turned off) and for controlling the input signal levels into the receiver. The received levels are kept below saturation levels, typically with a clutter AGC in search and a target AGC in single-target track, to prevent spurious signals, which degrade performance, from being generated.

Clutter Positioning. A voltage-controlled oscillator (VCO), usually part of the stable local oscillator (stalo), is used to heterodyne main-beam clutter to zero frequency, or dc. With the clutter at dc the in-phase (I) and quadrature (Q) channel amplitude and phase-balance requirements are eased, as the images resulting from unbalance also fall near dc and can be filtered out along with the main-beam clutter.

Transmit Pulse Suppressor. Further attenuation of transmitter leakage is provided by the transmit pulse suppressor in the receiver IF, which is a gating device.

Signal Processing. The analog output of the receiver is downconverted to baseband (dc) via quadrature mixing. The in-phase and quadrature signals are passed through a matched filter and converted to digital words by an analog-to-digital (A/D) converter. Following the A/D is typically a delay-line clutter canceler and doppler filter bank for main-beam clutter rejection and coherent integration. The filter bank is usually realized by using the fast Fourier transform
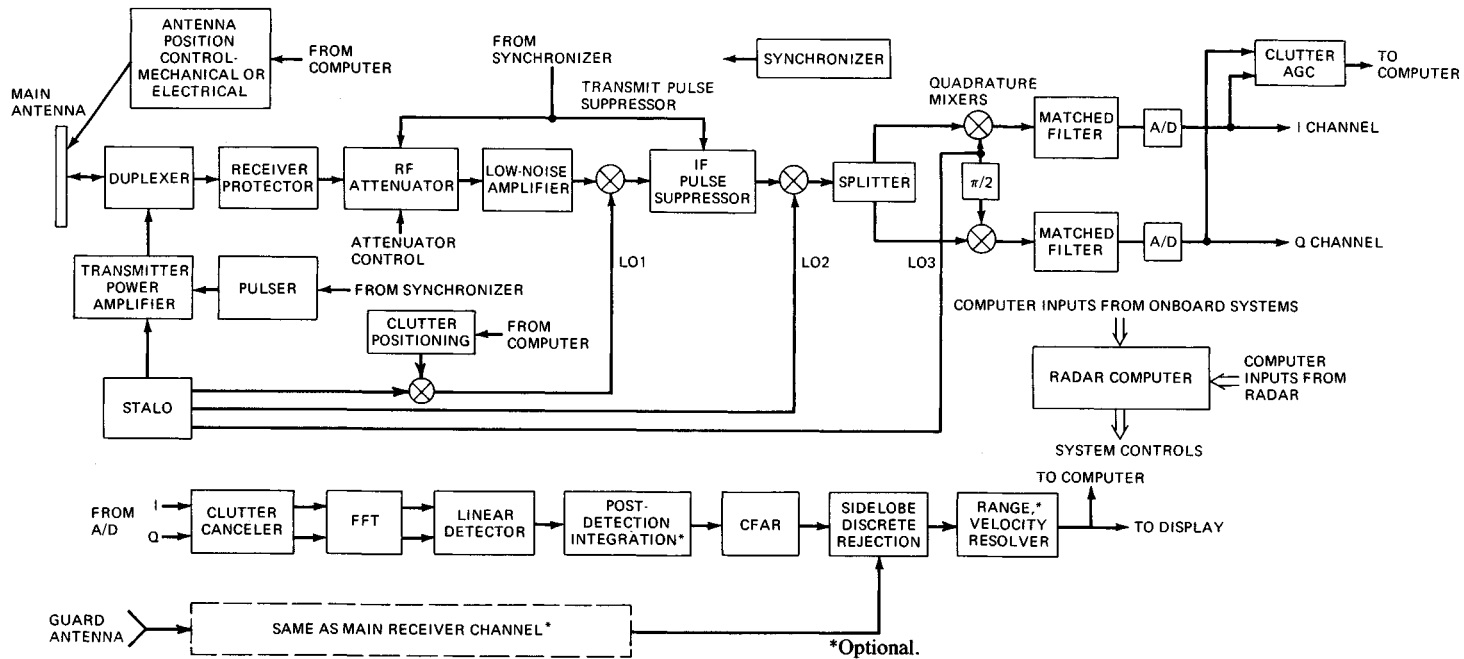
FIG. 17.6 Typical pulse doppler radar configuration.

17.8

(FFT) or by the discrete Fourier transform (DFT) for a small number of filters. Appropriate weighting is employed to reduce the filter sidelobes.

The voltage envelope at the output of the FFT is formed by using an I/Q combining approximation. Postdetection integration (PDI) may be used where each range-gate–doppler-filter output is linearly summed over several coherent looks. The PDI output is compared with a detection threshold determined by a constant-false-alarm-rate (CFAR)[17–20] process.

Following the CFAR is the sidelobe discrete rejection logic, discussed in Sec. 17.2, and the range and velocity ambiguity resolvers (if used). The final detection outputs are passed to the radar display and computer.

17.2 PULSE DOPPLER CLUTTER

General. Clutter returns from various scatterers have a strong influence on the design of a pulse doppler radar as well as an effect on the probability of detection of point targets. Clutter scatterers include terrain, both ground and water, rain, snow, and chaff. Since the antennas generally used in pulse doppler radars have a single, relatively high-gain main beam, main-beam clutter may be the largest signal handled by the radar when in a down-look condition, which is a principal reason for the use of medium- and high-PRF pulse doppler radars. The narrow beam limits the frequency extent of this clutter to a relatively small portion of the doppler spectrum. The remainder of the antenna pattern consists of sidelobes which result in sidelobe clutter. This clutter is generally much smaller than the main-beam clutter but covers much more of the frequency domain. The sidelobe clutter from the ground directly below the radar, the altitude line, is frequently large owing to a high reflection coefficient at steep grazing angles, the large geometric area, and the short range. Range performance is degraded for targets in the sidelobe clutter region wherever the clutter is near or above the receiver noise level. Multiple PRFs may be used to move the target with respect to the clutter, thus avoiding completely blind ranges or blind frequencies due to high clutter levels. This relative motion occurs owing to the range and doppler foldover. If one PRF folds sidelobe clutter and a target to the same apparent range and doppler, a sufficient change of PRF will separate them.

Ground Clutter in a Stationary Radar. When the radar is fixed with respect to the ground, both main-beam and sidelobe clutter returns occur at zero-doppler offset, the transmit frequency. The sidelobe clutter is usually small compared with main-beam clutter as long as some part of the main beam strikes the ground. The clutter can be calculated as in a pulse radar, then folded in range as a function of the PRF.

Ground Clutter in a Moving Radar. When the radar is moving with a velocity V_R, the clutter is spread over the frequency domain as illustrated in Fig. 17.2 for the special case of horizontal motion. The foldover in range and doppler is illustrated in Fig. 17.7 for a medium-PRF radar where the clutter is
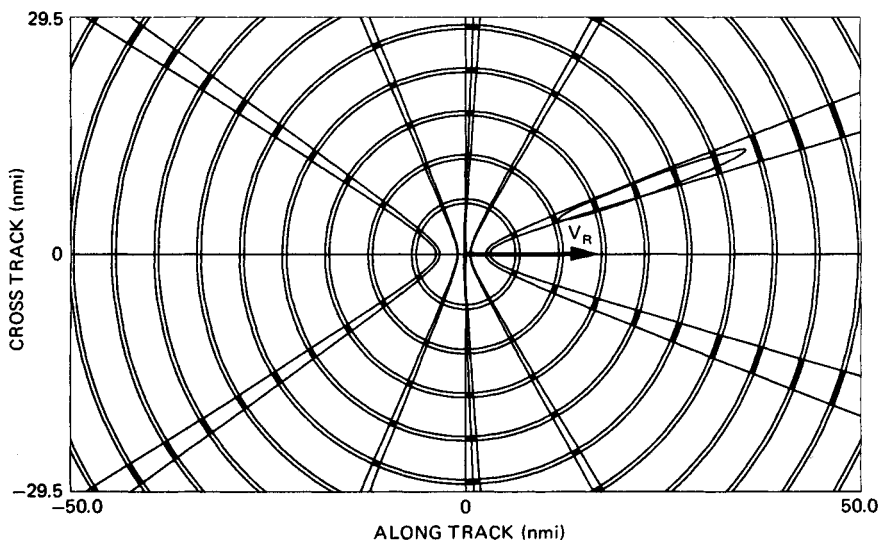
FIG. 17.7 Plan view of range-gate and doppler filter areas. Radar altitude, 10,000 ft; velocity, 1000 kn to right; dive angle, 10°; radar wavelength, 3 cm; PRF, 15 kHz; range-gate width, 6.67 μs; gate, 4; doppler filter, at 2 kHz; bandwidth, 1 kHz; beamwidth, 5° (circular); main-beam azimuth, 20°; depression angle, 5°.

ambiguous in both range and doppler. The radar platform is moving to the right at 1000 kn with a dive angle of 10°. The narrow annuli define the ground area that contributes to clutter in the selected range gate. The five narrow hyperbolic bands define the area that contributes to clutter in the selected doppler filter. The shaded intersections represent the area that contributes to the range-gate–doppler-filter cell. Each area contributes clutter power dependent on antenna gain in the direction of the area and the reflectivity of the area.

The main beam illuminates the elliptical area to the left of the ground track. Since this area lies entirely within the filter area, the main-beam clutter falls within this filter, and all other filters receive sidelobe clutter. Five range annuli are intersected by the main-beam ellipse; so the main-beam clutter in this range gate is the vector sum of the signals received from all five areas. Owing to this high degree of range foldover, all range gates will have approximately equal clutter.

If the main beam were scanned 360° in azimuth, the main-beam clutter would scan in frequency so that it would appear in the selected filter 10 times (twice for each hyperbolic band). In between, the filter would receive sidelobe clutter from all darkened intersections.

Clutter Return: General Equations. The clutter-to-noise ratio from a single clutter patch with incremental area dA at a range R is

$$C/N = \frac{P_{av} \, G_T \, G_R \, \lambda^2 \, \sigma^0 \, dA}{(4\pi)^3 \, R^4 \, L_c \, k \, T_s \, B_n} \tag{17.2}$$

where P_{av} = average transmit power
λ = operating wavelength
σ^0 = clutter backscatter coefficient
L_c = losses applicable to clutter
G_T = transmit gain in patch direction
G_R = receive gain in patch direction
k = Boltzmann's constant = 1.38054×10^{-23} W/(Hz/K)
T_s = system noise temperature, K
B_n = doppler filter bandwidth

The clutter-to-noise ratio from each radar resolution cell is the integral of Eq. (17.2) over the doppler and range extent of each of the ambiguous cell positions on the ground.[21-25] Under certain simplified conditions, the integration can be closed-form[25] while numeric integration may be used generally.

Sidelobe Clutter. The entire clutter spectrum can be calculated for each range gate by Eq. (17.2) if the antenna pattern is known in the lower hemisphere. In preliminary system design, the exact gain function may not be known, so that one useful approximation is that the sidelobe radiation is isotropic with a constant gain of G_{SL}.

Sidelobe Discretes. An inherent characteristic of airborne pulse doppler radars is that echoes from large objects on the ground (discretes), such as buildings, may be received through the antenna sidelobes and appear as though they were smaller moving targets in the main beam. This is a particularly severe problem in a medium-PRF radar, where all-aspect target performance is usually desired, as these returns compete with targets of interest. In a high-PRF radar, there is little if any range region clear of sidelobe clutter, such that the sidelobe clutter portion of the doppler spectrum is often not processed (since target detectability is severely degraded in this region). Further, in a high-PRF radar, especially at higher altitudes, the relative amplitudes of the distributed sidelobe clutter and the discrete returns are such that the discretes are not visible in the sidelobe clutter.

The apparent radar cross section (RCS), σ_{app}, of a sidelobe discrete with an RCS of σ is $\sigma_{app} = \sigma\, G_{SL}^2$, where G_{SL} is the sidelobe gain relative to the main beam. The larger-size discretes appear with a lower density than the smaller ones, and a model commonly assumed at the higher radar frequencies is as shown in Table 17.3. Thus, as a practical matter 10^6 m^2 discretes are rarely present, 10^5 m^2 sometimes, and 10^4 m^2 often.

Two mechanizations for detecting and eliminating false reports from sidelobe discretes are the guard channel and postdetection sensitivity time control (STC). These are discussed in the paragraphs which follow.

TABLE 17.3 Discrete Clutter Model

Radar cross section, m^2	Density, per mi^2
10^6	0.01
10^5	0.1
10^4	1

Guard Channel.   The guard channel mechanization compares the outputs of two parallel receiving channels, one connected to the main antenna and the second to a guard antenna, to determine whether a received signal is in the main beam or the sidelobes.[26-28] The guard channel uses a broad-beam antenna that (ideally) has a pattern above the main-antenna sidelobes. A range-cell, doppler-filter by range-cell, doppler-filter comparison is made of the returns in both channels. Sidelobe returns are rejected (blanked) when they are larger in the guard receiver, and main-lobe returns are passed without blanking since they are larger in the main receiver.

A block diagram of a guard channel mechanization is shown in Fig. 17.8. After the CFAR circuits (which ideally would be identical in both channels), there are three thresholds: the main channel, guard channel, and main-to-guard-ratio threshold. The detection logic of these thresholds is also shown in Fig. 17.8.

The blanking which occurs because of the main-guard comparison affects the detectability in the main channel, the extent of which is a function of the threshold settings. The threshold settings are a tradeoff between false alarms due to sidelobe returns and detectability loss in the main channel. An example is shown in Fig. 17.9 for a nonfluctuating target, where the ordinate is the probability of detection in the final output and the abscissa is the signal-to-noise ratio (SNR) in the main channel. The quantity B^2 is the ratio of the guard channel SNR to the main channel SNR and is illustrated in Fig. 17.10. B^2 is small for a target in the main beam and large, 0 dB or so, for a target at the sidelobe peaks. In the example shown, there is a 0.5 dB detectability loss due to the guard blanking for targets in the main beam.

Ideally, the guard antenna gain pattern would exceed that of the main antenna at all angles in space (except for the main beam) to minimize detections through the sidelobes. If not, however, as illustrated in Fig. 17.10, returns through the sidelobe peaks above the guard pattern have a significant probability of detection in the main channel and would represent false detections.

Postdetection STC.   A second approach to blanking sidelobe discretes is the postdetection STC,[29] the logic of which is shown in Fig. 17.11. Basically, the CFAR output data is correlated (resolved) in range 3 times. Each correlator calculates unambiguous range using M out of the N sets of detection data (e.g., three detections required out of eight PRFs). No doppler correlation is used since the doppler is ambiguous. The results of the first two correlations are used to blank all outputs which are likely to be sidelobe discretes from the final range correlator. Here, three range correlators are used in which the first, the A correlator, resolves the range ambiguities within some nominal range, say, 10 nmi, beyond which sidelobe discretes are not likely to be detected. A second correlator, the B correlator, resolves the range ambiguities out to the same range, but before a target can enter the B correlator, its amplitude is thresholded by a range-varying threshold (the STC threshold). A range-cell by range-cell comparison is made of the correlations in the A and B correlators, and if a range gate correlates in A and not in B, that gate is blanked out of the third correlator, the C correlator. The C correlator resolves the range ambiguities within the maximum range of interest.

The principle behind the postdetection STC approach is illustrated in Fig. 17.12, where the return of a target in the main beam and a large discrete target in the sidelobes is plotted versus unambiguous range (that is, after the range ambiguities have been resolved). Also shown are the normal CFAR threshold and the STC threshold versus range. As is evident, a discrete return in the sidelobes is
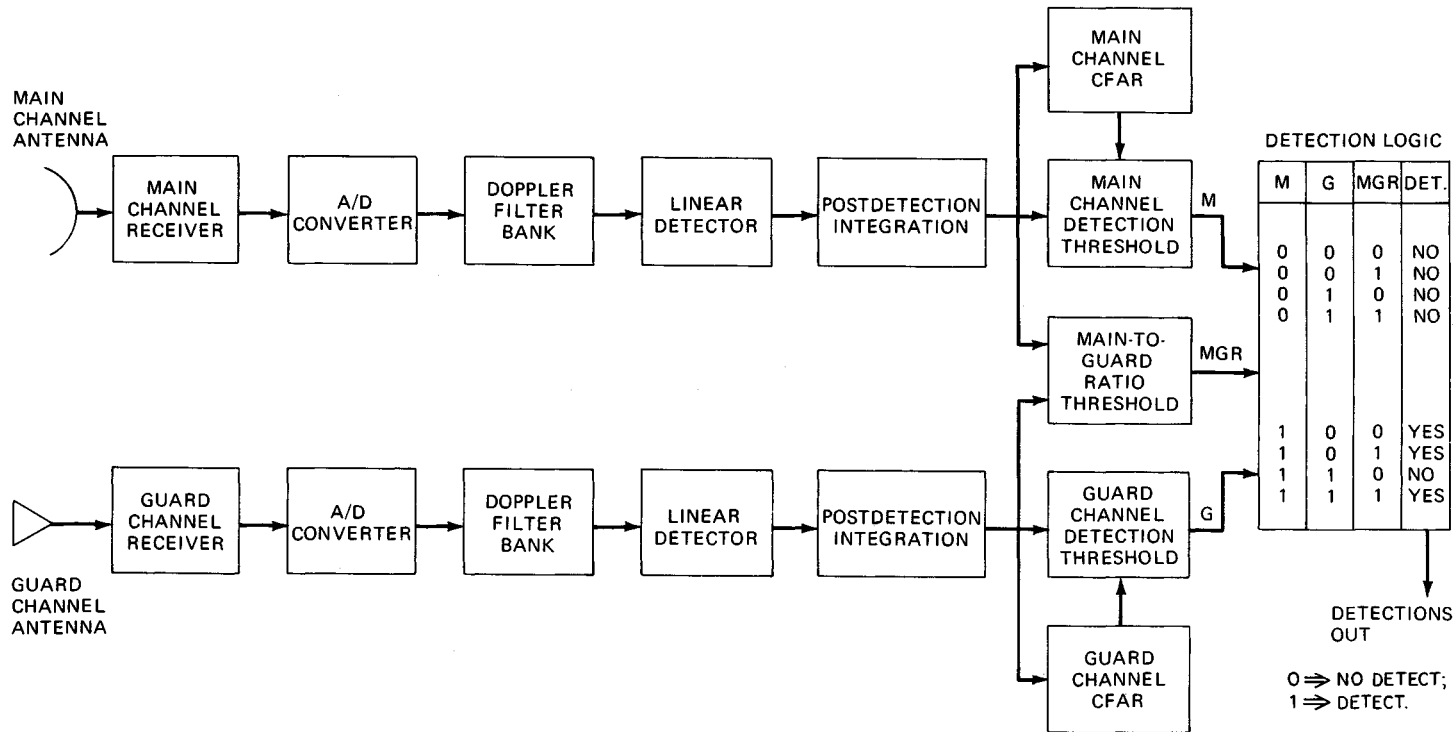
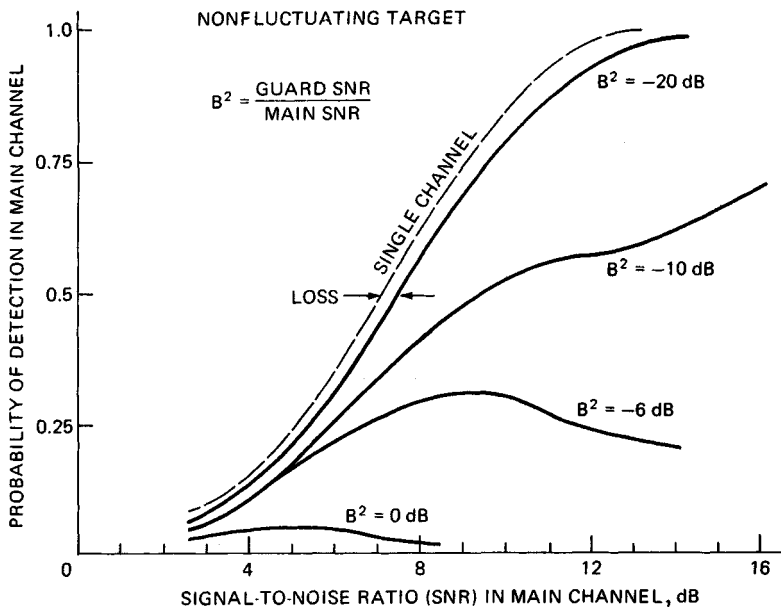FIG. 17.8 Two-channel sidelobe blanker.

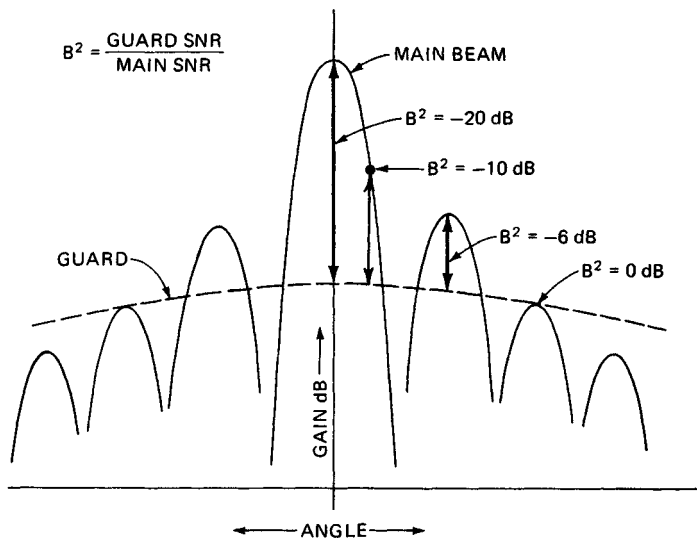**FIG. 17.9** Probability of detection versus signal-to-noise ratio with a guard channel.
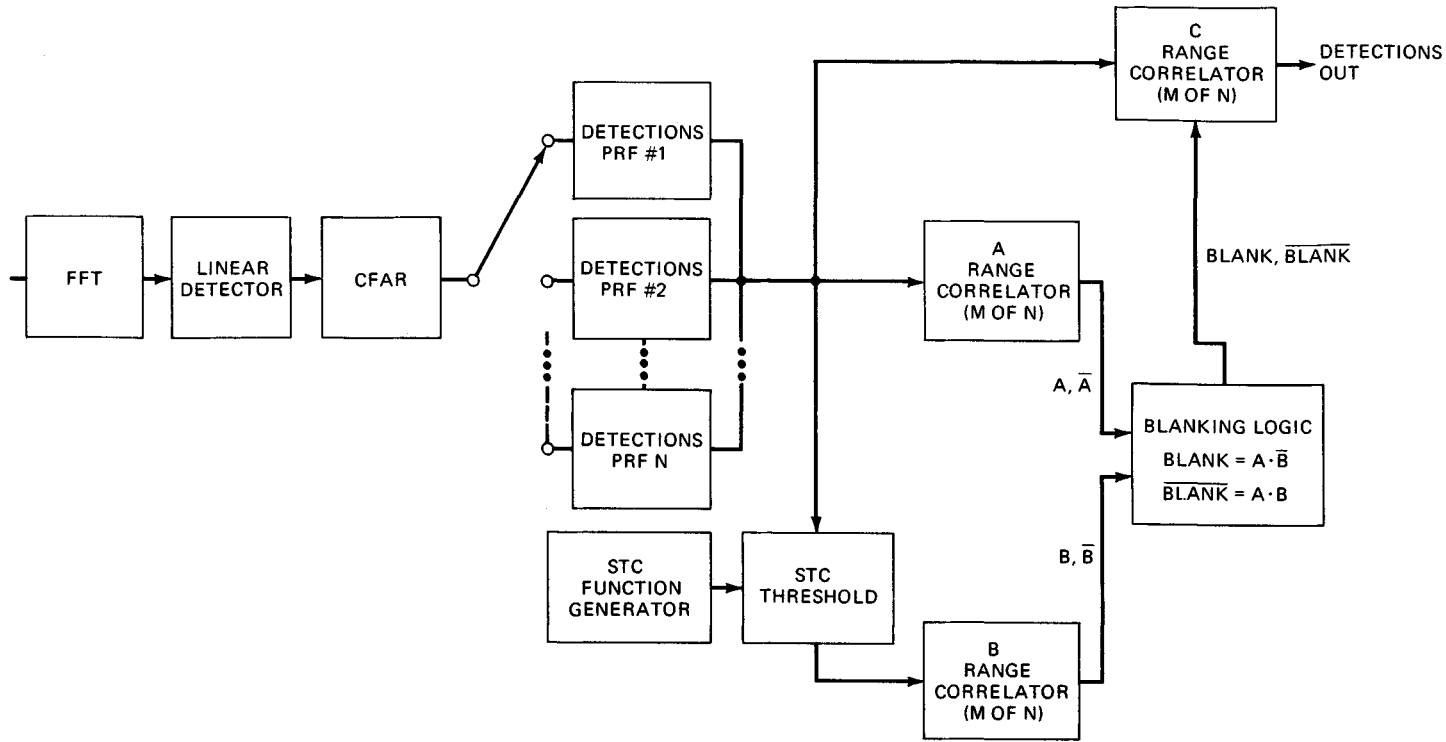

FIG. 17.10 Main and guard antenna patterns.

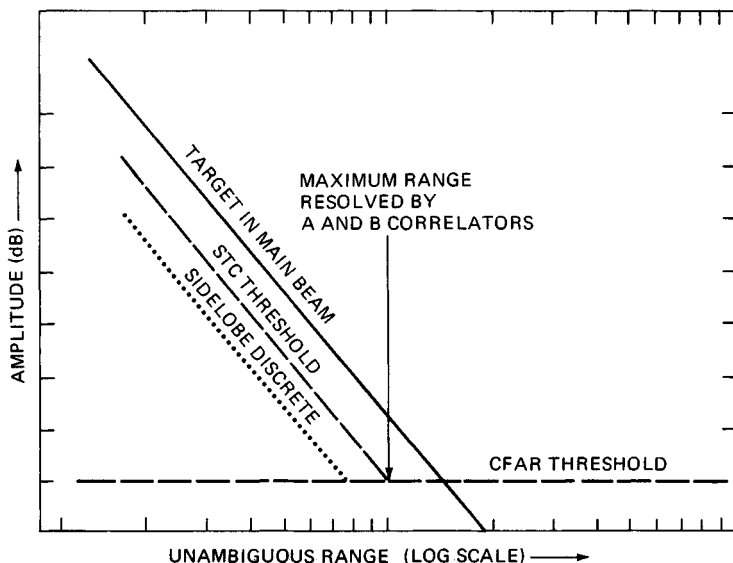FIG. 17.11 Single-channel sidelobe blanker.

FIG. 17.12 Postdetection STC levels.

below the STC threshold, and a return in the main beam is above the threshold, such that the sidelobe discrete can be recognized and blanked from the final output but the target will not be blanked.

Main-Beam Clutter. The main-beam clutter-to-noise power can be approximated from Eq. (17.2) by substituting the intersected area for dA and summing over all intersections within the main beam.[30]

$$\frac{C}{N} = \frac{P_{av}\lambda^2 \; \theta_{az} \; (c\tau/2)}{(4\pi)^3 \; L_c \; K \; T_s \; B_n} \sum \frac{G_T \; G_R \; \sigma^0}{R^3 \cos \alpha} \tag{17.3}$$

The summation limits are the lower and upper edges of the smaller of the transmit and receive beams and

where θ_{az} = azimuth one-half power beamwidth, rad
τ = compressed pulsewidth
α = grazing angle at clutter patch

The remaining terms are as defined following Eq. (17.2).

Main-Beam Clutter Filtering. In a pulse doppler radar utilizing digital signal processing, main-beam clutter is rejected by either a combination of a delay-line clutter canceler followed by a doppler filter bank or by a filter bank with low filter sidelobes. In either case, the filters around the main-beam clutter are blanked to minimize false alarms on main-beam clutter.

The choice between these options is a tradeoff of quantization noise and com-

plexity versus the filter-weighting loss. If a canceler is used, filter weighting can be relaxed over that with a filter bank alone, since the canceler reduces the dynamic-range requirements into the FFT (if the main-beam clutter is the largest signal). Without a canceler, heavier weighting is needed to reduce sidelobes to a level so that the filter response to main-beam clutter is below the thermal-noise level. This weighting increases the filter noise bandwidth and hence increases the loss in signal-to-noise ratio.

The improvement factor for a DFT filter[31] is given by

$$I(K) = \frac{\left[\sum_{n-0}^{N-1} A_n^2\right]}{\sum_{n=0}^{N-1} \sum_{m=0}^{N-1} A_n A_m \exp\{-2[\pi(n-m)\,\sigma_c\,T]^2\} \cos[2\pi K(n-m)/N]} \qquad (17.4)$$

where A_i = DFT weight, $0 \le i \le N - 1$
N = number of points in DFT
σ_c = standard deviation of clutter spectrum
K = filter number ($K = 0$ is dc filter)
T = interpulse period

Here, the improvement factor for a filter (versus the more common definition applied to a delay-line canceler) is defined as the ratio of the total clutter power input to the filter to the clutter residue in that filter. Expressed another way, the improvement factor is the ratio of the clutter power out of a filter if it were centered over the clutter, and the clutter width reduced to zero, to the power out of the filter in actual operation.[32,33] Figure 17.13 shows the improvement factor of a 256-point, Dolph-Chebyshev weighted FFT as a function of the clutter width for various filter numbers in the filter bank.

If the main beam is pointed below the horizon and is greater than a beamwidth from 0° azimuth, the 6 dB clutter width due to platform motion Δf is

$$\Delta f = \frac{2V_R}{\lambda} \theta_B \sin \psi_0 \qquad (17.5)$$

where V_R = radar ground speed
ψ_0 = main-beam angle relative to velocity vector
θ_B = 3 dB one-way antenna beamwidth, rad
λ = RF wavelength

Clutter-Transient Suppression. When the PRF is changed for multiple-PRF ranging, or the slope is changed in linear FM ranging, or the RF carrier is changed, the transient change in the clutter return may cause degradation unless it is properly handled.[34] Since the clutter is usually ambiguous in range in a pulse doppler radar, the clutter power increases at each interpulse period (IPP) as clutter return is received from longer-range ambiguities, until the horizon is reached. This phenomenon is called *space charging*. Note that although an increasing number of clutter returns are received during the charging period, the vector sum may actually decrease owing to the random phase relations of the returns from different patches.
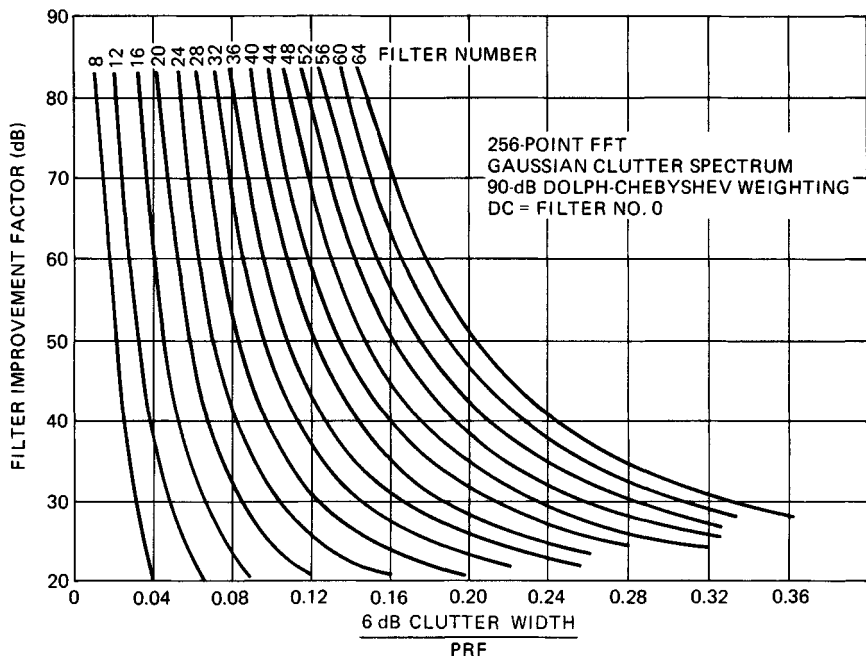
FIG. 17.13   Filter improvement factor versus clutter width.

If a clutter canceler is used, the output cannot begin to settle to steady-state value until space charging is complete. Some settling time must be allowed before signals are passed to the filter bank. Therefore, the coherent integration time available at each look is reduced from the total look time by the sum of the space charge time and the transient settling time. The canceler settling time can be eliminated by "precharging" the canceler with the steady-state input value.[35] This is done by changing the canceler gains so that all delay lines achieve their steady-state values on the first IPP of data.

If no canceler is used, signals can be passed to the filter bank after the space charge is complete, so that the coherent integration time is the total look time minus the space charge time.

Altitude-Line Clutter Filtering.   The reflection from the earth directly beneath an airborne pulse radar is called altitude-line clutter. Because of specular reflection over smooth terrain, the large geometric area, and the relatively short range, this signal can be large. It lies within the sidelobe clutter region of the pulse doppler spectrum.

Because it can be much larger than diffuse sidelobe clutter and has a relatively narrow spectral width, altitude-line clutter is often removed by either a special CFAR which prevents detection of the altitude line or by a tracker-blanker which removes these reports from the final output. In the case of the tracker-blanker, a closed-loop tracker is used to position range and velocity gates around the altitude return and blank the affected range-doppler region.

17.3 TIME GATING

Time gating of the receiver permits blanking of transmitter leakage and its noise sidebands, elimination of excess receiver noise from competing with the signal, range gating for target tracking, and true range measurement, provided the ambiguity can be resolved.

Transmitted-Pulse Suppression. One major advantage of pulse doppler over CW systems is the time blanking of transmitter leakage so that receiver sensitivity is not degraded owing to saturation effects or to noise sidebands on the transmitter.

Harmonic Frequencies. Extreme care is required to prevent spurious signals from appearing in the system output. For example, if a 30-MHz IF receiver is being gated at a 110-kHz PRF, the 272d harmonic of the gating transient will fall at 29.92 MHz and the 273d at 30.03 MHz. Either of these harmonics may be within the doppler passband and therefore appear in the output. Although high-order harmonics of the gating transient are relatively small, they may be large compared with the signal since gating occurs early in the receiver.

Gating and Synchronization. One solution to the gating-harmonic problem is the use of balanced gating circuits and synchronization of the IF passband and the PRF so that the PRF harmonics all fall outside the useful portion of the passband. An alternative solution is to heterodyne the clutter to a frequency that is a multiple of the PRF so that the PRF harmonics are rejected with the clutter. However, such solutions preclude a variable-PRF system other than in discrete, accurately known steps.

Although synchronization of the PRF and the IF passband is usually necessary, synchronization at RF is not usually required. The harmful harmonics are of a much higher order and therefore are much smaller. In addition, the RF gating transients are usually further reduced in amplitude by the IF gating circuit.

Transmitter Leakage. The on-off ratio required for the overall transmitter blanking circuits is fairly large (more than can be obtained readily at RF without excessive insertion loss). Thus a combination RF and IF blanking system is usually employed. The transmitter leakage through the blanking circuits can be allowed to be as large as main-beam clutter if there is zero-doppler filtering to remove it. Alternatively, it must be a fraction of the noise power in a detection filter if there is no such filtering.

Range Gating. Range gating eliminates excess receiver noise from competing with the signal and permits target tracking and range measurement. Range gating is very similar to transmitted-pulse suppression. In a single-channel 0.5-duty-cycle system, one pulse-suppressor circuit serves both functions. In multiple-range-gated systems the range gates can serve both functions. If one circuit serves both functions, the on-off ratio must be adequate for pulse suppression, whereas if two are used, the range gate does not need as much rejection.

17.4 RANGE-AMBIGUITY RESOLUTION

Several methods of ranging are commonly employed in high PRF, while medium PRF is usually confined to multiple discrete PRF ranging.

High-PRF Ranging. Range-ambiguity resolution in high PRF is performed by modulating the transmitted signal and observing the phase shift of the modulation on the return echo. Modulation methods include varying the PRF, either continuously or in discrete steps; varying the RF carrier, with either linear or sinusoidal FM; or some form of pulse modulation such as pulse-width modulation (PWM), pulse-position modulation (PPM), or pulse-amplitude modulation (PAM). Of these modulation techniques, PWM and PPM may have large errors because of clipping of the received modulation by eclipsing or straddling (discussed in Sec. 17.7), and PAM is difficult to mechanize in both the transmitter and the receiver. Consequently, they will not be further considered here.

Multiple Discrete PRF Ranging. Ranging by use of several (usually two or three) fixed PRFs involves sequential measurement of the ambiguous range in each PRF, followed by comparison of the measurements to eliminate ambiguities.[36,37] Figure 17.14 illustrates the principle of multiple-PRF ranging for a two-PRF, high-PRF radar. The PRFs are chosen to have a common submultiple frequency $1/T_u$. If the transmitted-pulse trains are compared in a coincidence detector, the common submultiple frequency is obtained. Similarly, if the received gates are compared in a coincidence detector, the same submultiple frequency shifted in time by the target range delay T_r is obtained. Measuring the time delay between the two sets of coincidence pulses yields the true target range. If desired, a three-PRF system can be mechanized similarly. The advantage obtained is the increased unambiguous range achievable.

FIG. 17.14   Principle of two-PRF ranging.

In a surveillance radar a number of receiver gates are used to detect targets that may appear at any range within the interpulse period. Figure 17.15 illustrates a common method of spacing the gates for the general case where the gate spacing τ_s, the gate width τ_g, and the transmitted pulse τ_t are all unequal. Selecting $\tau_g > t_s$ reduces the range-gate straddle loss but increases the possibility of range ghosts. Selecting $\tau_t = \tau_g$ maximizes range performance.

FIG. 17.15 Example of three range gates equally spaced in the interpulse period.

The PRFs are usually related by the ratios of closely spaced, relatively prime integers m_1, m_2, and m_3, as indicated in Table 17.4. Thus a three-PRF system using the seventh, eighth, and ninth submultiples of the range-gate clock frequency $f_c = 1/\tau_s$ as PRFs yields an unambiguous range of $7 \times 9 = 63$ times that of the middle PRF alone.

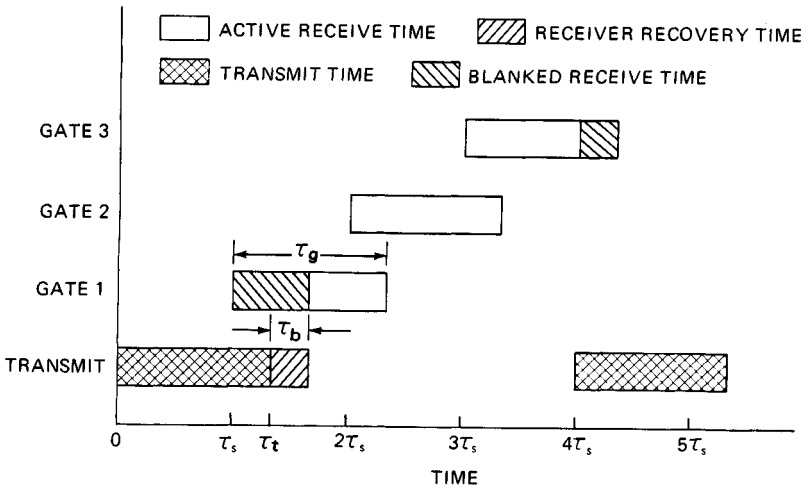**TABLE 17.4**   Multiple-PRF Ranging Parameters

Item	Two-PRF	Three-PRF
Ranging parameters: $m_1 > m_2 > m_3$	m_1, m_2	m_1, m_2, m_3
Number of range-gated channels	$m_1 - 1$	$m_1 - 1$
PRFs		
$\quad f_{R1}$	$1/m_1\tau_s$	$1/m_1\tau_s$
$\quad f_{R2}$ ($f_{R3} > f_{R2} > f_{R1} \geq f_{Rmin}$)	$1/m_2\tau_s$	$1/m_2\tau_s$
$\quad f_{R3}$		$1/m_3\tau_s$
Unambiguous range (R_{max})	$m_2c/2f_{R1}$	$m_2m_3c/2f_{R1}$
Transmitter duty cycle, d	$\tau_t f_{R2}$	$\tau_t f_{R3}$
Ratio of highest and lowest PRF	m_1/m_2	m_1/m_3

NOTE: m_1, m_2, m_3 must be relatively prime integers.
  τ_t = transmitted pulsewidth
  τ_g = range-gate width
  τ_b = blanking width due to receiver recovery
  τ_s = range-gate spacing
  f_c = range-gate clock = $1/\tau_s$

Figure 17.16 shows the maximum unambiguous range as a function of the minimum PRF, f_{Rmin}, and the ranging parameter m_1, for the case where m_1, m_2, m_3 are consecutive integers. It is usually desirable to keep m_1 in the region from about 8 to 50. Thus the unambiguous range of a two-PRF system is seen to be rather limited, whereas three PRFs give much larger ranges. Some of the considerations influencing the choice of m_1 to this range are as follows:
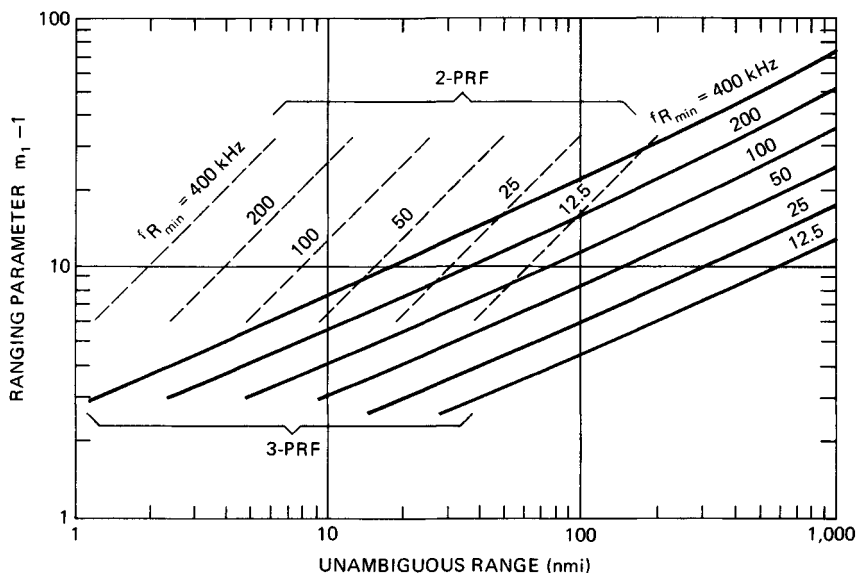
FIG. 17.16 Unambiguous range for two- and three-PRF ranging systems as a function of ranging parameters, $m_1 - 1$, and minimum value of PRF for the case where m_1, m_2, m_3 are consecutive integers and m_1 is odd.

1. To minimize hardware, m_1 should be small since a maximum of $m_1 - 1$ range gates must be processed.

2. The probability of eclipse in at least one PRF is about $3/m_1$ for a three-PRF system, and so m_1 should be at least eight or higher since range cannot be measured if any PRF is eclipsed.

3. To get a long unambiguous range, m_1 should be large.

4. For good range resolution, τ_T must be small, which requires that m_1 be large. (Target range change during the dwell limits the minimum τ_t.)

5. To minimize the transmitter duty cycle and hence the average-power variation between PRFs, m_1 should be relatively large.

The Chinese remainder theorem is one means for calculating the true range from the several ambiguous measurements in a range-while-search system.[38] This approach permits a unique direct computation of the true-range cell number R_c from the three ambiguous-range cell numbers A_1, A_2, and A_3 (or two numbers for a two-PRF system). (The cell number is the range expressed in units of the pulse width and ranges from 0 to $m_i - 1$.) The theorem for a three-PRF system is expressed by the congruence

$$R_c \quad (C_1 A_1 + C_2 A_2 + C_3 A_3) \quad (\text{modulo } m_1 m_2 m_3) \tag{17.6}$$

The smallest value of R_c that satisfies Eq. (17.6) is the remainder of the term within parentheses when divided by $m_1 m_2 m_3$ as many times as possible. There-

fore, $0 \leq R_c < m_1 m_2 m_3$. The constants C_1, C_2, and C_3 are related to m_1, m_2, and m_3 by the congruences

$$C_1 = b_1 m_2 m_3 \equiv 1 \ (\text{modulo } m_1) \tag{17.7}$$

$$C_2 = b_2 m_1 m_3 \equiv 1 \ (\text{modulo } m_2) \tag{17.8}$$

$$C_3 = b_3 m_1 m_2 \equiv 1 \ (\text{modulo } m_3) \tag{17.9}$$

where b_1 is the smallest positive integer which, when multiplied by $m_2 m_3$ and divided by m_1, gives unity as the remainder (and similarly for the other b's).

Once m_1, m_2, and m_3 have been chosen, the range can be computed from Eq.(17.6) by using the C values and the ambiguous-range cell numbers (A_1, A_2, A_3) in which the target is detected. For example, if $m_1 = 7$, $m_2 = 8$, $m_3 = 9$, then $b_1 = 4$, $b_2 = 7$, $b_3 = 5$, and the range is $R_c = (288A_1 + 441A_2 + 280A_3) \ (\text{modulo } 504)$. If the target is in the first gate after the transmit pulse, $A_1 = A_2 = A_3 = 1$ and $R_c = (288 + 441 + 280) \ (\text{modulo } 504) = 1$. An alternative to the Chinese remainder theorem is either a hard-wired correlator or a special-purpose computer that accepts detections from all PRFs and outputs all double or triple correlations.

Continuously Variable PRF Ranging. In a single-target tracking radar, the range ambiguity can be resolved by varying the PRF so that the target return is centered in the interpulse period. A high duty cycle, 0.333 to 0.5, may be used. Range R can then be calculated by

$$R = -\frac{\dot{R} f_R}{\dot{f}_R} \tag{17.10}$$

This method of range measurement has poor accuracy because of the errors involved in measuring the derivatives. An advantage of this technique is that the target return is never eclipsed by the transmitter pulse, thus improving tracking. It has a disadvantage, however, in that PRF harmonics can appear within the doppler band as spurious signals.

Linear-Carrier FM. Linear frequency modulation of the carrier can be used to measure range, especially in range-while-search applications. The modulation and demodulation to obtain range are the same as used in CW radar, but the transmission remains pulsed.

Assume that the dwell time is divided into two periods. In the first period, no FM is applied, and the doppler shift of the target is measured. In the second period, the transmitter frequency is varied linearly at a rate $\dot{f}$ in one direction. During the round-trip time to the target, the local oscillator has changed frequency so that the target return has a frequency shift, in addition to the doppler shift, that is proportional to range. The difference in the frequency Δf of the target return in the two periods is found, and the target range calculated from

$$R = \left| \frac{c \Delta f}{2 \dot{f}} \right| \tag{17.11}$$

The problem with only two FM segments during a dwell time is that, with more than a single target in the antenna beamwidth, range ghosts result. For example, with two targets present at different dopplers, the two frequencies observed during the FM period cannot be unambiguously paired with the two frequencies observed during the no-FM period. Thus, typical high-PRF range-while-search radars use a three-segment scheme in which there are no-

FM, FM-up, and FM-down segments. The range is found by selecting returns from each of the three segments that satisfy the relations

$$f_1 < f_0 < f_2 \tag{17.12}$$

$$f_1 + f_2 = 2f_0 \tag{17.13}$$

where $f_0, f_1,$ and f_2 are the frequencies observed during the no-FM, FM-up, and FM-down segments, respectively. The range then is found from Eq. (17.11), where

$$\Delta f = f_2 - f_0 \quad \text{or} \quad (f_2 - f_1)/2 \quad \text{or} \quad f_0 - f_1 \tag{17.14}$$

An example is shown in Fig. 17.17.

Target	A	B
Range, nmi	10	20
Doppler frequency, kHz	21	29
FM shift, kHz	3	6
Observed frequencies		
f_0, no FM, kHz	21	29
f_1, FM up, kHz	18	23
f_2, FM down, kHz	24	35

Possible sets which satisfy the relations shown in Eqs. (17.12) and (17.13) are:

f_1	f_0	f_2	$2f_0$	$f_1 + f_2$	Target?	Range, nmi
18	21	24	42	42	Yes	10
18	21	35	42	53	No	
18	29	35	58	53	No	
23	29	35	58	58	Yes	20

FIG. 17.17 Three-slope FM ranging example. There are two targets, A and B; $\dot{f}$ = FM slope = 24.28 MHz/s.

If more than two targets are encountered during a dwell time, ghosts again result, as only $N - 1$ simultaneously detected targets can be resolved ghost-free where N is the number of FM slopes. This is not a severe problem in practice, however, for multiple targets in a single beamwidth are usually a transient phenomenon.

The accuracy of the range measurement improves as the FM slope increases since the observed frequency differences can be more accurately measured. However, the FM slope is limited by clutter-spreading considerations since during the FM periods the clutter is smeared in frequency and can appear in frequency regions normally clear of clutter. Range accuracies on the order of 1 or 2 mi can be reasonably achieved.

Sinusoidal-Carrier FM. This method is similar to that sometimes used in CW radar but retains the pulse transmission. It is particularly useful for tracking, ei-

ther continuously or in a pause-to-range mode (discussed in Sec. 17.5). It is not suitable for range-while-search because of the relatively long time required to measure the phase shift of the sinusoidal modulation.

Medium-PRF Ranging.   Multiple discrete PRF ranging, as discussed for high PRF, is also used for medium PRF except that the PRF selection criterion differs.[13] The technique of using closely spaced PRFs can be extended to medium PRF by employing three groups of three closely spaced PRFs, the groups being widely spaced to improve doppler visibility. The center PRF in each group is called the *major* PRF, and the adjacent ones the *minor* PRFs. Ranging is accomplished by requiring a detection in the major PRF and its adjacent minor PRFs and is effectively a detection criterion of exactly three detections out of three opportunities. This approach is attractive from a ghosting standpoint but suffers owing to the poor doppler visibility that results from having only three PRFs visible.

A better technique for medium PRF is to use seven or eight PRFs which cover nearly an octave in frequency and to require detections in at least three of these to declare a target report. The advantage is that doppler visibility is better than with the major-minor approach, and hence better range performance in sidelobe clutter is achieved (where some PRFs may be obscured by clutter). However, it is more susceptible to ghosting owing to the high doppler visibility. This problem is mitigated by also resolving the doppler ambiguities and using the true doppler for correlation to reject ghosts.

The basic accuracy of multiple-PRF ranging is on the order of the range-gate size (150 m/μs), but this can be improved to a fraction of the gate width by amplitude centroiding.

17.5   TARGET TRACKING

Target tracking can be performed on either a single target, using more or less conventional angle, range, and velocity tracking servo loops, or on multiple targets, using track-while-scan.

Single-Target Tracking.   Angle tracking can be identical to a conventional pulse radar using monopulse, sequential lobing, or conical scan. Monopulse is more difficult to mechanize because of the problem of phase and amplitude matching of the multiple receiver channels, but the problem can be mitigated by using self-calibration routines controlled by the radar computer.

In a low-duty-cycle radar, range tracking is similar to pulse radar tracking in that split-gate tracking is used. In a high-duty-cycle radar, continuously variable PRF ranging or linear-FM ranging may be used. In a pulse doppler radar, the tracked range is usually ambiguous, so that provisions must be made to track through multiple interpulse periods and during eclipse (that is, when the target return overlaps the transmitted pulse).

Velocity (or doppler) tracking in a pulse doppler radar is carried out by forming a centroid on the target's doppler return in the filter bank. A closed-loop tracker then positions a doppler window around the tracked target such that returns which differ in doppler by more than a predetermined value are discarded by the tracker. In medium PRF, the PRF has to be adjusted to keep the doppler return away from the main-beam clutter notch as well as to avoid range eclipse.

Tracking through Eclipse. Because of the range ambiguities in medium and high PRF, the radar must cope with the loss of target each time that it passes through eclipse. Automatic tracking systems might recycle to the search mode if eclipse is not recognized and preventive measures taken.

The multiple-PRF true-ranging system is the most positive solution. Once true range has been determined so that the range ambiguity is resolved, PRF switching eliminates eclipsing. The onset of eclipse is detected by the range tracker by noting when the range gate begins to overlap the transmitted pulse. Then, before eclipse occurs, the PRF is switched to one of the other values. One of these values is certain to be uneclipsed, owing to the synchronization and relative PRF values. Since tracking is carried out in true range, no transient occurs and eclipse-free tracking continues indefinitely.

The continuously variable PRF system also permits eclipse-free tracking, but because of the spurious-signal problem it has not received much favor.

Other ranging systems do not permit eclipse-free tracking. FM ranging is not accurate enough to predict when eclipsing is about to occur. If the range is not accurately known, there is no way to anticipate an eclipse. In this case, an after-the-fact eclipse detection is made. A target-presence-detector circuit notes the absence of a signal and assumes that this is due to an eclipse. This circuit then commands the PRF to change value in an attempt to bring the target out of eclipse.

The problems with this approach are that target scintillation can cause PRF cycling and that there is no accurate way to predict which PRF will prevent eclipse. The latter problem can be reduced, if crude FM range data is available, by selecting the PRF from groups of PRFs, each group having values appropriate for a particular region of ranges. This reduces the time required in searching for an uneclipsed PRF.

Multiple-Target Tracking. Multiple-target tracking can be accomplished in several ways. One, track-while-scan, is to use the normal search mode with FM or multiple-PRF ranging and store the range, angle, and doppler of the reported detections in the computer. These detections are then used to form track files. The antenna scans in a normal search pattern, and a scan-to-scan correlation is made on the detections which update the track files. Although tracking accuracies are less than can be achieved in a single-target track, multiple targets can be tracked simultaneously over a large volume in space.

A second method of multiple-target tracking, pause-while-scan, particularly applicable to electronic scan antennas, is to scan in a normal search pattern, pause on each search detection, and enter a single-target track mode for a brief period. The advantage is that the resulting range, angle, and doppler measurements are more accurate than those made with a scanning antenna, but the time to search a volume in space is increased.

17.6 DYNAMIC-RANGE AND STABILITY REQUIREMENTS

Dynamic Range. Dynamic range as discussed here is the linear region above thermal noise over which the receiver and signal processor operate before any saturation (clipping) or gain limiting occurs. If saturations occur,

spurious signals which degrade performance may be generated. For example, if main-beam clutter saturates, spurious frequencies can appear in the doppler passband normally clear of main-beam clutter and generate false-target reports. An AGC function is often employed to prevent saturations on either main-beam clutter in search or the target in single-target track mode. If saturations do occur in a range gate during an integration period, an option in a multiple-range-gated system is simply to blank detection reports from that gate.

The most stressing dynamic-range requirement is due to main-beam clutter when searching for a small low-flying target. Here, full sensitivity must be maintained in the presence of the clutter to maximize the probability of detecting the target.

The dynamic-range requirement of a pulse doppler radar, as determined by main-beam clutter, is a function not only of the basic radar parameters such as power, antenna gain, etc., but of radar altitude above the terrain and the radar cross section (RCS) of low-flying targets. As an example, Fig. 17.18 shows the maximum clutter-to-noise ratio (C/N_{max}) which appears in the ambiguous-range interval, i.e., after range folding, for a medium-PRF radar as a function of radar altitude and the range of the main-beam center. Note that the quantity plotted is the rms value of the clutter-to-noise ratio. A pencil-beam antenna pattern is as-
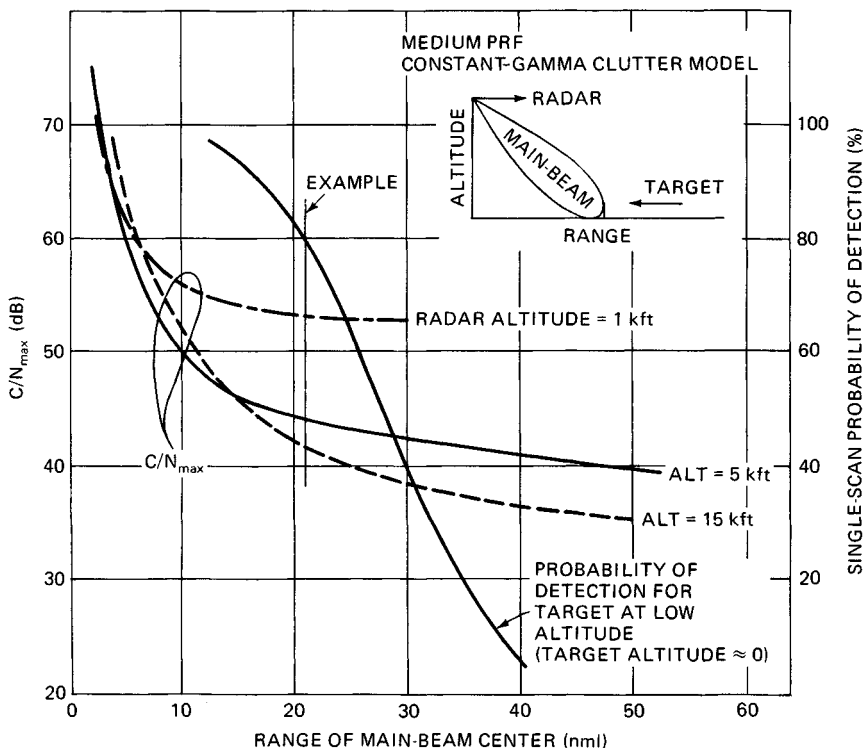

FIG. 17.18 Dynamic-range example.

sumed. At the longer ranges (small look-down angles), the clutter decreases with increasing altitude since range folding is less severe owing to less of the main beam intersecting the ground. At the shorter ranges, clutter increases with altitude since the clutter patch size on the ground increases. While Fig. 17.18 is for a medium-PRF radar, similar curves result for a high-PRF radar.

Also shown in Fig. 17.18 is the single-scan probability of detection P_d versus range for a given RCS target in a receiver with unlimited dynamic range. If it is desired to have the low-flying target reach at least, say, an 80 percent P_d before any gain limiting occurs, the dynamic-range requirement due to main-beam clutter is 53 dB at 1000 ft, 44 dB at 5000 ft, and 41 dB at 15,000 ft for this example. As is evident, the higher the desired probability of detection or the lower the radar altitude, the more dynamic range that is required. Further, if the specified target RCS is reduced, the dynamic-range requirement for the same desired P_d increases as the P_d-versus-range curve in Fig. 17.18 shifts to the left.

In a PD radar using digital signal processing, the dynamic range is most often limited by the A/D converters. The maximum signal level relative to thermal noise that can be processed linearly is related to the number of amplitude bits in the A/D by

$$\frac{S_{\max}}{N} = 20 \log \left(\frac{2^{\text{NAD}} - 1}{\text{noise}} \right) \qquad (17.15)$$

where $S_{\max}/N$ = maximum input level relative to noise, dB
NAD = number of amplitude bits in the A/D
noise = rms thermal-noise level at the A/D, quanta

From the relationships described above and assuming that the A/D limits the dynamic range, the A/D size can now be determined. An additional factor, that of a margin to allow for main-beam clutter fluctuations above the rms value, also needs to be considered. Since main-beam clutter time fluctuation statistics are highly dependent on the type of clutter being observed, such as sea clutter or clutter from an urban area, and are generally unknown, a value of 10 to 12 dB above the rms value is often assumed for the maximum level. Thus, the required number of amplitude bits in the A/D converter as determined by the main-beam clutter is

$$\text{NAD} \geq \text{CEIL} \left[\frac{(C/N)\text{max (dB)} + \text{fluc margin (dB)} + 20 \log (\text{noise})(q)}{6} \right] \qquad (17.16)$$

where CEIL is the next larger integer.

For the example cited in Fig. 17.18 where the maximum C/N is 53 dB at a 1000-ft altitude, and with a fluctuation margin of 10 dB and thermal noise at 1.414 quanta, the A/D requires at least 11 amplitude bits (plus a sign bit).

Stability Requirements. To achieve the theoretical clutter rejection and target detection and tracking performance of a pulse doppler system, the reference frequencies, timing signals, and signal-processing circuitry must be adequately stable.[39–42] In most cases, the major concern is with short-term stability rather than long-term drift. Long-term stability mainly affects velocity or range accuracy or spurious signals (due to PRF harmonics) but is relatively

easy to make adequate. Short-term stability refers to variations within the round-trip radar echo time or during the signal integration time. The most severe stability requirements relate to the generation of spurious modulation sidebands on the main-beam clutter, which can appear as targets to the target detection circuitry. Thus, the ratio of main-beam clutter to system noise measured at the receiver output (C/N), including the fluctuation margin as discussed above, is the predominant parameter that determines stability requirements. However, at low spurious modulation frequencies, other constraints may become limiting.

Types of Spurious Modulation. The various spurious modulations that can appear on the received signal (clutter or target return) include both carrier and pulse modulation.

Carrier modulation can be amplitude modulation (AM), common FM, or independent FM. Common FM refers to identical modulation on both the transmitted signal and the receiver local-oscillator signal; independent FM appears on only one or the other or in the receiver following the first mixer.

Pulse modulation can be common pulse-position modulation (PPM), independent pulse-width modulation (PWM), or pulse droop. In these cases, common modulation refers to in-phase modulation on both the transmitter pulse and the receiver range gate or transmitter blanking gate. Independent modulation occurs if only one of these pulses is affected. Common PWM does not usually occur. However, if it does, it has requirements similar to those of common PPM. Also, pulse-amplitude modulation (PAM) can occur but is usually negligible when the other requirements are satisfied.

Sinusoidal Modulations. Any of these types of modulation may be caused by a sinusoidal disturbance, such as power supply ripple, line-frequency pickup, or sinusoidal vibration. Discrete sidebands at the modulation frequency and possibly higher harmonics will be introduced on the clutter and target signals. Since the pulse doppler receiver is basically a spectral analyzer, the radar requirements are most readily defined in terms of the allowable level of these modulation sidebands.

The predominant effect of these sidebands depends on the sideband frequency. For sideband frequencies greater than f_{min}, the sidebands on clutter signals fall outside the clutter rejection filter, where f_{min} is the minimum frequency separation of a detection filter from the edge of the main-beam clutter. This spread clutter must be kept below receiver noise; otherwise, it either will be detected as a target or will desensitize the receiver at these frequencies.

For sideband frequencies between $B_n/2$ and f_{min}, the concern is with either a target SNR loss or generation of false targets, where B_n is the receiver predetection-filter bandwidth. The SNR loss results from the sideband energy falling outside the detection filter. The false-target effect is due to modulation sidebands on a strong target appearing to the detection filters as weak targets.

For sideband frequencies below the reciprocal of the postdetection integration time T_1, sidebands per se cease to be of concern. However, the instantaneous-signal-frequency excursion should not be greater than the predetection bandwidth during the integration time, or a SNR loss results. Also, the signal amplitude should not be modulated significantly from one integration period to the next, or the sensitivity could change.

Sidebands in the immediate vicinity of the antenna lobing frequency or range track jitter frequency must be small enough to prevent excessive tracking error or noise.

TABLE 17.5 Allowable Deviation of Pulse or Carrier Sinusoidal Modulation as a Function of Modulating Frequency

Modulation frequency	Criterion	Factor Q	PAM-δ AM-M	Common FM δ_F	Independent FM δ_F	Independent PWM δ_W	Common PPM δ_P	Independent PPM δ_P
0 to $1/T_I$	Signal constant for T_I	0.1	$2Q$	. . . .	. . . .	$2\pi d_{min}Q$	$\dfrac{\tau d_{min}Q}{\pi f_m T_c}$	$2\pi d_{min}Q$
		$B_n/4\pi f_m T_I$	. . . .	$Q/\pi f_{mTc}$	$2Q$			
$1/T_I$ to $1/\pi T_c$	Target *SNR* loss	$(0.1i!)^{1/i}$	No requirement	$Q/\pi T_c$	$2f_mQ$	No requirement (for natural sampling)		
	Clutter spreading	$[j!\sqrt{K_s/(C/N)}]^{1/j}$		$Q/\pi T_c$	$2f_mQ$			
$f_L - f_{bw}$ to $f_L + f_{bw}$	Tracking error	$K_M\sigma_E/\sqrt{2}(\theta \ or \ \tau)$	$2Q$	No requirement	No requirement	$2\pi d_{min}Q$	$\tau d_{min}Q$	$2\pi d_{min}Q$
$1/\pi T_c$ to $B_n/2$	Target *SNR* loss	. . . .	No requirement	$f_m(0.1i!)^{1/i}$	$2f_m(0.1i!)^{1/i}$	No requirement (for natural sampling)		
	Clutter spreading	$[j!\sqrt{K_s/(C/N)}]^{1/j}$		f_mQ	$2f_mQ$			
$B_n/2$ to f_{min}	Target *SNR* loss	. . . .	No requirement	$f_m(0.1i!)^{1/i}$	$2f_m(0.1i!)^{1/i}$	No requirement (for natural sampling)		
	Clutter spreading	$[j!\sqrt{K_{s/(C/N)}}]^{1/j}$		f_mQ	$2f_mQ$			

$5B_n$ to f_{min}	False targets	$\sqrt{K_s/(\max SNR)}$	$2Q$	$f_m Q$	$2f_m Q$	$2\tau Q$	τQ	$2\tau Q$
f_{min} and higher	Clutter spreading	$\sqrt{K_s/(C/N)}$	$2Q$	$f_m Q$	$2f_m Q$	$2\tau Q$	τQ	$2\tau Q$

M = peak fractional carrier amplitude modulation

δ_F = peak carrier frequency deviation, Hz

f_m = modulating frequency, Hz

T_c = two-way delay for main-beam clutter, s

δ_W = peak pulse-width deviation, s

d_{min} = minimum target signal duty cycle when partly eclipsed (say, $\tau f_R/5$)

δ_p = peak pulse-position deviation, s

K_s = safety factor of modulation power sidebands relative to system noise ($K_s \leq 1$)

f_L = tracking subcarrier frequency, Hz

f_{bw} = tracking-loop noise bandwidth, Hz

K_M = modulation sensitivity (fractional modulation/ beamwidth or pulse-width error)

σ_E = rms tracking error due to modulation sidebands

θ = antenna beamwidth

$\max SNR$ = maximum target power SNR that does not cause automatic gain control or limiting

i = integer part of $[(B_n/2) + f_m]/f_m$

j = integer part of $(f_{min} + f_m)/f_m$

δ_Δ = peak fractional pulse-amplitude modulation

Applying all these constraints to the various types of modulations expected gives the sinusoidal modulation allowances of Table 17.5 where 0.1 dB tolerable loss was assumed in *SNR*. The various modulation-frequency regions (not sideband frequencies) corresponding to the predominant sideband effects (i.e., the criterion column in Table 17.5) are listed. A factor Q for each region is indicated; it is related to the maximum allowable deviation indicated in other columns. For example, for independent pulse-width modulation, for a modulation frequency greater than f_{min}, the maximum allowable deviation is

$$\delta_w = 2\tau Q = 2\tau\left[\frac{K_s}{(C/N)max}\right]^{1/2} \tag{17.17}$$

for acceptable clutter spreading. The safety factor K_s assures that the clutter sidebands will be buried in receiver noise.

Each tabulated value assumes that only one source of modulation is present. If multiple modulations are expected, an appropriate reduction factor must be provided so that the composite sidebands do not exceed the tolerable value.

In the receiver following the main-beam clutter filter, the clutter-spreading requirements are not germane. The *SNR* and false-target considerations then become the limiting factors at high-sideband frequencies as well as low-sideband frequencies.

Narrowband Noise. Although the requirements in Table 17.5 relate to a single-frequency sinusoidal modulation, they can be interpreted for narrowband-noise modulation. For this interpretation, the listed modulation values represent $\sqrt{2}$ times the allowable rms noise modulation referenced to a bandwidth of B_n. This interpretation is fairly good for modulating frequencies much greater than $B_n/2$, but for lower frequencies it is only a rough guide.

PPM and PWM. The pulse-position and pulse-width values are based on the assumption of natural sampling,[43] as is normally the case. In natural sampling, the deviation of the pulse edge is determined by the amplitude of the modulating signal at the time of occurrence of the pulse edge. Because of the range delay of target clutter signals and the range gating, PPM can be converted to PWM, which generates much larger sidebands. Most clutter signals are partially eclipsed or partially outside the range gate; therefore, the position of one edge of the pulse in the receiver is determined by the transmitted pulse, and the other edge is determined by the range gate or transmitter blanking pulse. Thus the original PPM can be converted into PWM as a function of modulating frequency and time delay to the clutter.

The deviation requirements in Table 17.5 were derived for the worst case, where the two common modulating signals are 180° out of phase or one edge of the received clutter pulse is completely eclipsed in the independent case.

Frequency Modulation. Common FM permits relaxed modulation requirements at low frequencies but 6 dB more severe requirements at high frequencies compared with independent FM.[44] This effect is caused by the range delay of the clutter. Since the transmitter and the receiver local oscillator are frequency-modulated in synchronism, the deviation of the IF difference signal is dependent on the range delay.

Droop. Although it does not cause new spectral sidebands and therefore was not included in Table 17.5, pulse droop on the transmitter modulator pulse is also of interest. This is because of the high phase-modulation sensitivity of traveling-wave tubes and klystrons typically used as RF amplifiers. A linear droop of the modulating voltage will serrodyne the RF signal, shifting the peak of the spectral

envelope relative to the RF carrier frequency and reducing the useful signal power when passed through a filter matched to the pulse width. For small droop this loss is given by

$$\text{Fractional power loss} = \frac{1}{3}\left[\frac{\pi}{3.6}K_\phi\frac{\Delta V}{V}\right]^2 \tag{17.18}$$

where K_ϕ = transmitter phase sensitivity (degrees phase change/percent voltage)
$\Delta V/V$ = fractional voltage droop on modulator pulse

Pulse-to-Pulse Random Modulation. In addition to the sinusoidal or narrowband-noise modulation, pulse-to-pulse random modulation may also be present. The predominant effect is clutter spreading noise into the detection filter. With the same notation as for Table 17.5, the factor Q is $[K_s f_R/(C/N)B_n]^{1/2}$, and the rms allowable fractional AM is equal to Q, as is the rms phase modulation (given in radians). The rms PPM or single-edge PWM allowable modulation (given in seconds) is τQ.

17.7 RANGE PERFORMANCE

Chapter 2 discusses the general radar range equation and the calculation of detection probability. This section extends those concepts to pulse doppler radars and includes a discussion of system losses and false-alarm probability. Generalized detection curves, which include multilook detection criteria, are presented.

Range Equation. In the doppler region where the signal does not fall in clutter, performance is limited only by system noise. The signal-to-noise ratio in the detection filter prior to postdetection integration for a target at range R is given by

$$SNR = \left(\frac{R_o}{R}\right)^4 \tag{17.19}$$

$$R_o = \left(\frac{P_A\,G_T\,G_R\,\lambda^2\,\sigma_T}{(4\pi)^3 k\,T_s\,B_n\,L}\right)^{1/4} \tag{17.20}$$

where R_o = range at which $S/N = 1$
σ_T = target radar cross section
L = losses applicable to the target

The remaining terms are as defined following Eq. (17.2).

System Losses. Some of the losses inherent in, but not necessarily unique to, pulse doppler radars which employ digital signal processing are discussed below.

Quantization Noise Loss. This loss is due to the noise added by the A/D conversion process and to truncation due to finite word lengths in the signal-processing circuits which follow.[45]

CFAR Loss. This is caused by an imperfect estimate of the detection threshold compared with the ideal threshold. The fluctuation in the estimate necessitates that the mean threshold be set higher than the ideal, hence a loss.

Doppler Filter Straddle Loss. This loss is due to a target not always being in the center of a doppler filter. It is computed by assuming a uniformly distributed target doppler over one filter spacing and is a function of the FFT sidelobe weighting.

Amplitude-Weighting Loss. This loss results from the increased noise bandwidth of the doppler filters that occurs because the filter sidelobe weighting. It can also be accounted for by an increase of the doppler filter noise bandwidth instead of as a separate loss.

Pulse Compression Mismatch Loss. This is caused by the intentional mismatching of the pulse compression filter to reduce the time (range) sidelobes.

Guard Blanking Loss. This is the detectability loss in the main channel caused by spurious blanking from the guard channel. (See Fig. 17.9.)

Eclipsing and Range-Gate Straddle Loss. Because of eclipsing, the value of R_o, given by Eq. (17.20), may fall anywhere between zero and a maximum value, depending on the exact location of the target return in the interpulse period. When the PRF is high, so that many range ambiguities occur, the target range delay may be considered to be random from scan to scan, with a uniform distribution over the interpulse period. An approximate measure of performance in this case is found by first computing a detection curve averaged over target ambiguous ranges from zero to the range corresponding to the interpulse period. The loss is equal to the increase in signal-to-noise ratio required to obtain the same probability of detection with eclipsing or straddle as in the case when the transmit pulse is received by a matched gate with no straddle. Since the detection curve changes shape, the loss depends on the probability of detection selected. A less accurate approximation compares the average signal-to-noise ratio over the interpulse period with the signal-to-noise ratio of the matched case. In the case of M contiguous range gates of width τ that occupy the entire interpulse period except for the transmitted pulse also of width τ, the average eclipsing and straddle loss on a signal-to-noise-ratio basis is

$$\text{Eclipse and straddle loss} = \frac{Y}{3(M + 1)} \qquad \tau_t = \tau_g \qquad (17.21)$$

where
$$
\begin{aligned}
Y_1 &= (1 - R)(2 + R) & M &= 1 \\
Y &= (1 - R)(1 - R + 2X) + 2 + 1.75(M - 2) & M &> 1, R \geq 0.618 \\
Y &= (1 - R)(1 + R + Z) + (Z - R)[Z(Z + X)] \\
&\quad + (1 - Z)[Z(Z + 1) + 1] + 1 + 1.75(M - 2) & M &> 1, R < 0.618 \\
Z &= 1/(1 + X) \\
X &= \sqrt{1 - R} \\
R &= \tau_b/\tau \\
\tau_b &= \text{width of first gate blanking} \\
\tau &= \text{width of transmitted pulse } \tau_t \text{ and receiver gate } \tau_g \\
M &= \text{number of contiguous gates}
\end{aligned}
$$

The loss is plotted in Fig. 17.19. Signals cannot be received during the time τ_b following each transmit pulse owing to slow shutoff of the transmitter or recovery of the duplexer and/or receiver-protector.
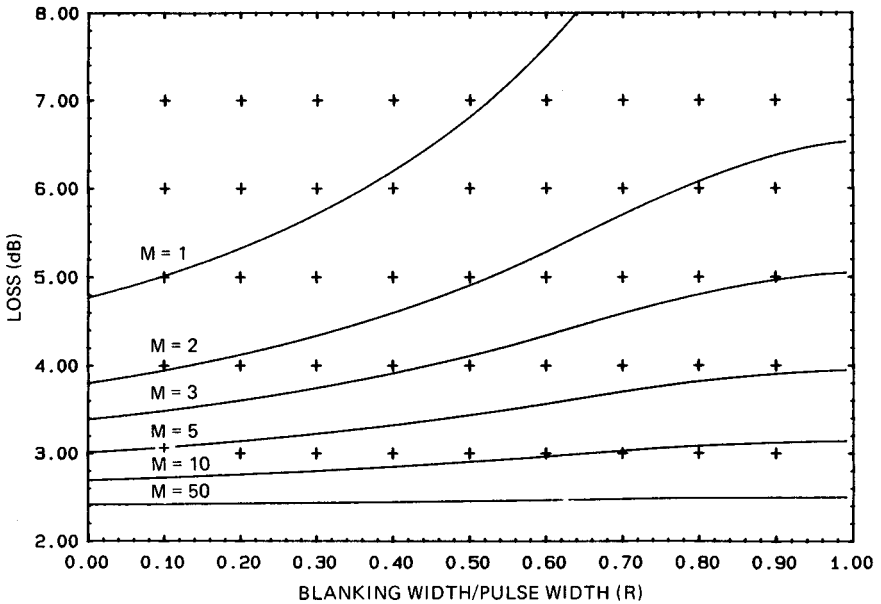
FIG. 17.19 Eclipsing and straddle loss for M contiguous range gates and equal transmitted pulse and range-gate widths as a function of the number of receive gates and blanking width.

Although Eq. (17.21) assumes contiguous range gates, the loss factor can be reduced by the use of overlapping gates at the expense of extra hardware and possibly more range ghosts.

Probability of False Alarm. PD radars often employ a multilook detection criterion to resolve range ambiguities such that during the time on target (dwell time) several PRFs are transmitted in successive looks and a threshold detection in more than one look is required for the radar to output a target report. For the case where a doppler filter bank in each range gate is used for coherent integration, possibly followed by a postdetection integrator, the probability of false alarm P_{FA} in each range gate–doppler filter required to obtain a given false report time T_{FR} is given approximately by

$$P_{FA} = \frac{1}{N_F}\left[\frac{0.693\ T_d}{\binom{n}{m}\ N_g\ T_{FR}}\right]^{1/m} \tag{17.22}$$

where N_F = number of independent doppler filters visible in the doppler passband (number of unblanked filters/FFT weighting factor)

n = number of looks in a dwell time

m = number of detections required for a target report (For example, 3 detections out of 8 PRFs is $m = 3$ and $n = 8$.)

T_d = total dwell time of the multiple PRFs including postdetection integration (if any) and any dead time

$\binom{n}{m}$ = binomial coefficient $n!/[m!(n - m)!]$

N_g = number of range gates in the output unambiguous-range interval (display range/range-gate size)

T_{FR} = false-report time [per Marcum's definition where the probability is 0.5 that at least one false report will occur in the false-report time (Ref. 46)]

Equation (17.22) is for the case where no doppler correlation is required for a target report. In the case where both range and doppler correlation are used, the required P_{FA} is

$$P_{FA} = \left[\frac{0.693 \, T_d}{\binom{n}{m} N_{fu} N_g T_{FR} W^{m-1}} \right]^{1/m} \qquad (17.23)$$

where N_{fu} = number of independent doppler filters in the unambiguous doppler region and W = width (in filters) of the correlation window applied to detections following initial detection.

Probability of Detection. The probability-of-detection curves presented in Chap. 2 have been extended to include multilook detection criteria and are presented in a generalized fashion after Ref. 47; that is, they are presented in terms of gR/R_o, where the g factor is a function of the number of pulses integrated noncoherently and the probability of false alarm. For coherent integration $N = 1$ and g becomes

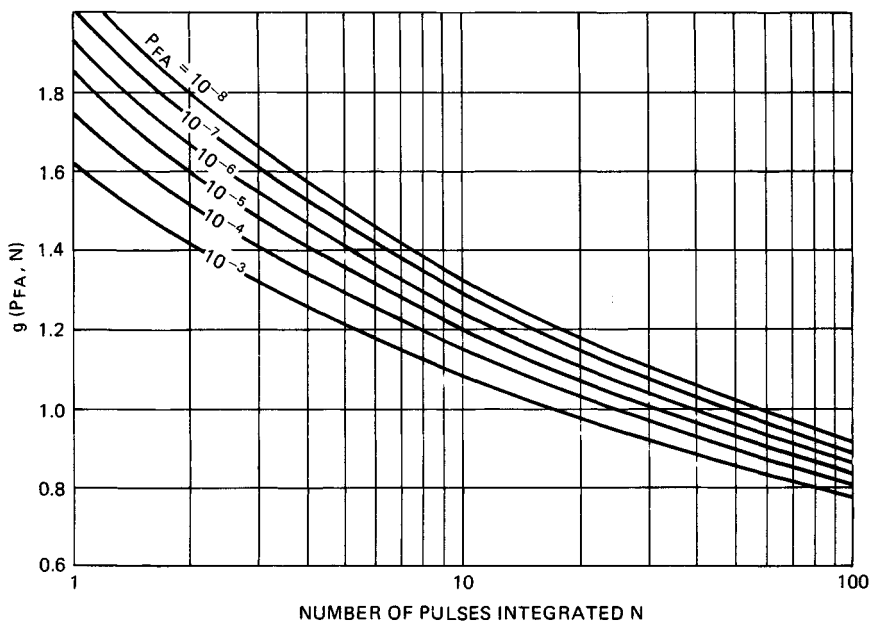$$g = [- \ell n(P_{FA})]^{1/4} \qquad (17.24)$$

FIG. 17.20 Swerling's g factor as a function of P_{FA} and N (after Ref. 47).

The g factor is plotted in Fig. 17.20 for various false-alarm probabilities and number of pulses integrated.

The generalized results are based on the realization that Marcum's curves[46] are very similar over a wide range of parameters; one can reasonably use a single universal Marcum curve as shown in Fig. 17.21. This is patterned after the universal curve presented in Ref. 47, except that here it is for a nonfluctuating target. It is accurate to within 1 dB over the entire range (and closer over most of the range) of integration samples N from 1 to 100, probability of false-alarm values P_{FA} from 10^{-3} to 10^{-8}, and probability from 1 to 99 percent. To use Fig. 17.21, a value of $g(P_{FA}, N)$ is first found from Fig. 17.20; this can then be used to convert gR/R_o values to R/R_o or signal-to-noise-ratio values.
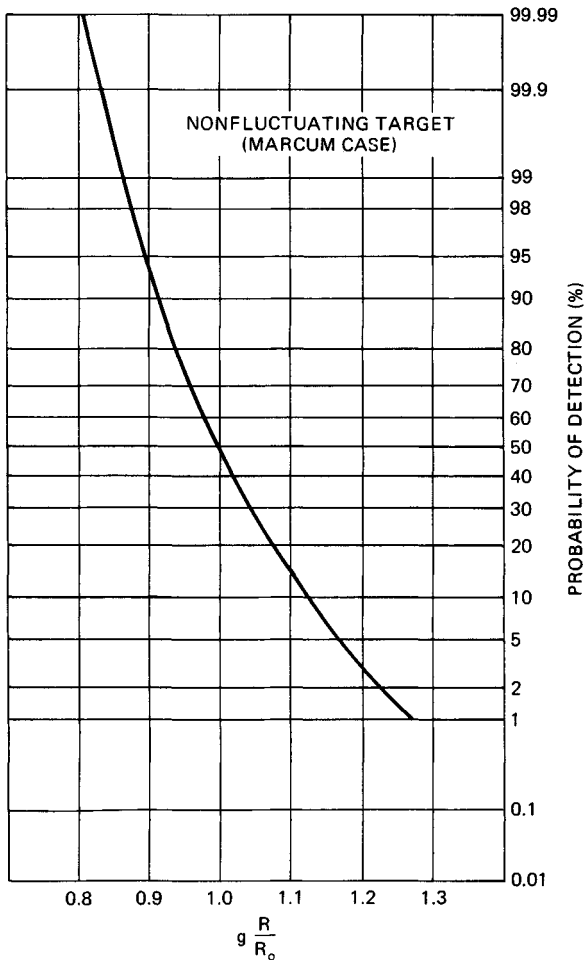

FIG. 17.21   Universal Marcum curve.

Generalized Curves.   By using the universal Marcum curve, several detection cases have been generated and are shown in Fig. 17.22. These are all for a Swerling Case 1 target in which the target amplitude fluctuates independently from scan to scan but is constant within the dwell time. No losses other than the fluctuation loss have been included in these curves, so that any losses such as range-gate straddle and eclipsing can be accounted for in the computation of R_o.

The Swerling Case 1 single-scan detection curves can be closely approximated by

$$P_d = P_{\mathrm{FA}}^{\left(\frac{1}{a+b\,SNR}\right)} \tag{17.25}$$

where P_d = single-scan detection probability
  P_{FA} = probability of false alarm
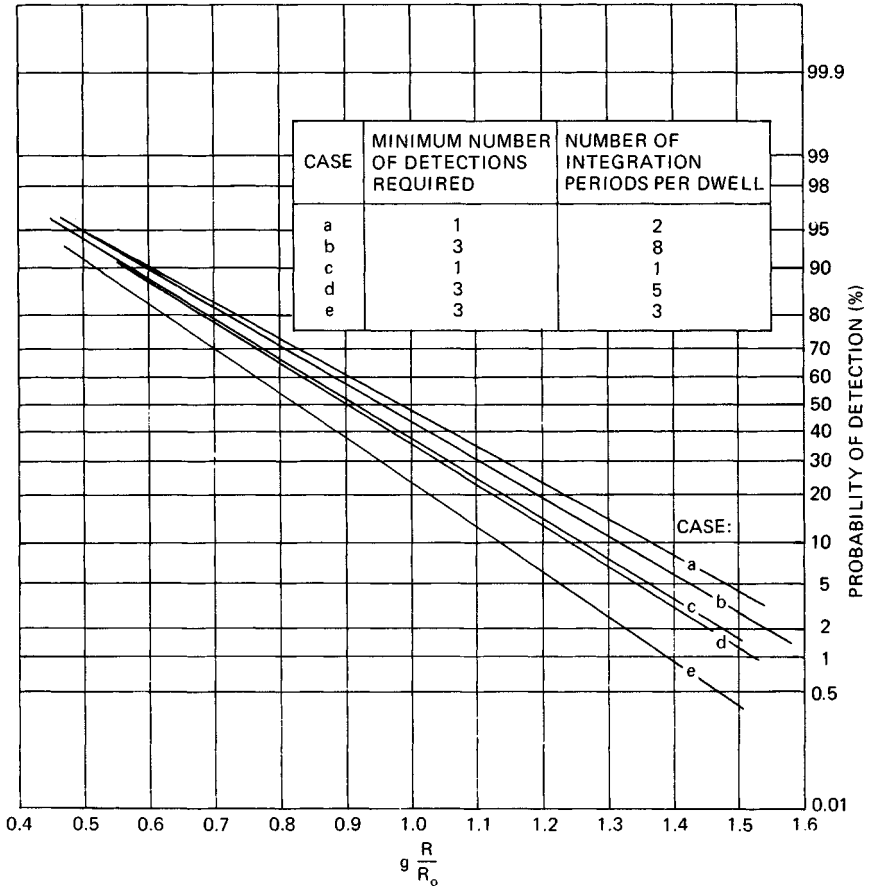 SNR = signal-to-noise ratio = $(R_o/R)^4$

FIG. 17.22   Generalized single-scan probability of detection for a scan-to-scan, Swerling Case 1, Rayleigh fluctuating target.

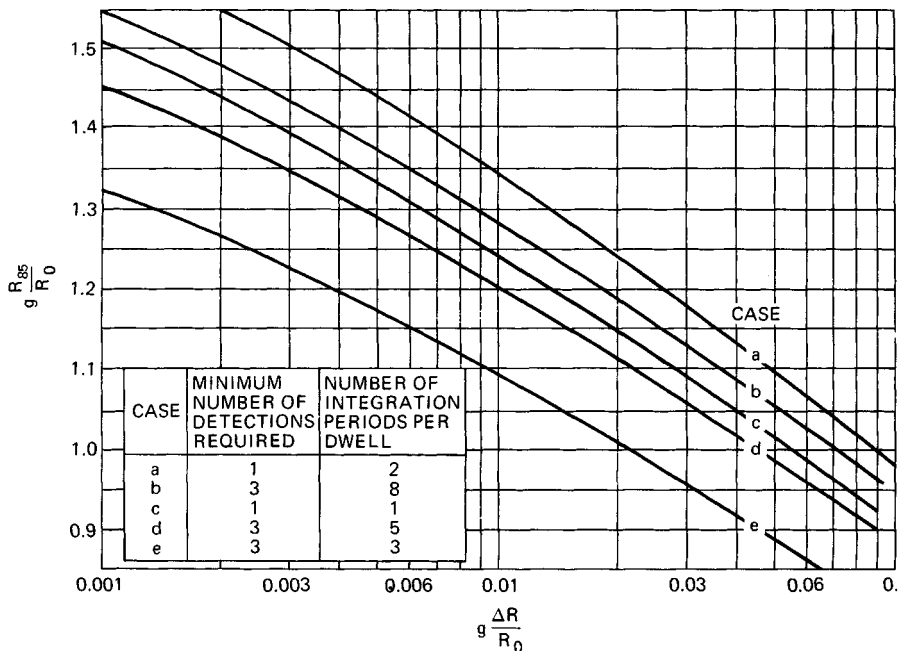| CASE	MINIMUM NUMBER OF DETECTIONS REQUIRED	NUMBER OF INTEGRATION PERIODS PER DWELL
a	1	2
b	3	8
c	1	1
d	3	5
e	3	3

FIG. 17.23 Generalized 85 percent cumulative probability of detection for scan-to-scan, Swerling Case 1, Rayleigh fluctuating target.

The constants a and b can be found by substitution, using two pairs of P_d and gR/R_o values from Fig. 17.22, converting gR/R_o to SNR, and solving the resultant simultaneous equations.

The cumulative probability of detection (probability of detecting the target at least once in k scans), Pc_k, is defined as

$$Pc_k = 1 - \prod_{i=1}^{k}[1 - P_d(i)] \qquad (17.26)$$

where $P_d(i)$ is the probability of detection on the ith scan. The cumulation may occur over a variable number of scans, such as when it begins at a range where $P_d(i)$ is approximately zero, or over a defined number of scans, where a 1-out-of-N acquisition criterion must be satisfied. The single-scan probability-of-detection curves shown in Fig. 17.22 have been used to compute the 85 percent cumulative probability of detection for the variable-scan case, shown in Fig. 17.23. ΔR is the change in range between successive scans for a fixed-velocity, radially moving target.

Clutter-Limited Case. The foregoing discussion assumed that the target fell in the noise-limited (i.e., clutter-free) part of the doppler band. If the target falls in the sidelobe clutter region, the range performance will be degraded, since the total power (system noise plus clutter) with which the target must compete is increased. The foregoing discussion can be applied to the sidelobe clutter region, however, by interpreting R_o as the range where the signal is equal to sidelobe clutter plus system

noise.[48–50] The CFAR loss may also be higher owing to the increased variability of the threshold when the clutter varies over the target detection region.

REFERENCES

1. Skolnik, M. I.: Fifty Years of Radar, *Proc. IEEE*, vol. 73, pp. 182–197, February 1985.

2. Perkins, L. C., H. B. Smith, and D. H. Mooney: The Development of Airborne Pulse Doppler Radar, *IEEE Trans.*, vol. AES-20, pp. 290–303, May 1984.

3. Clarke, J., D. E. N. Davies, and M. F. Radford: Review of United Kingdom Radar, *IEEE Trans.*, vol. AES-20, pp. 506–520, September 1984.

4. Moaveni, M. K.: Corrections to "Radio Interference in Helicopter-Borne Pulse Doppler Radars," *IEEE Trans.*, vol. AES-14, p. 688, July 1978.

5. Moaveni, M. K.: Radio Interference in Helicopter-Borne Pulse Doppler Radars, *IEEE Trans.*, vol. AES-14, pp. 319–328, March 1978.

6. Ringel, M. B., D. H. Mooney, and W. H. Long: F-16 Pulse Doppler Radar (AN/APG-66) Performance, *IEEE Trans.*, vol. AES-19, pp. 147–158, January 1983.

7. Skillman, W. A.: Utilization of the E-3A Radar in Europe, *Proc. Mil. Electron. Def. Expo '78*, Wiesbaden, Germany, 1978.

8. Skillman, W. A.: Microwave Technology, Key to AWACS Success, *Proc. IEEE MTT/S*, Boston, 1983.

9. Clarke, J.: Airborne Early Warning Radar, *Proc. IEEE*, vol. 73, pp. 312–324, February 1985.

10. Doviak, R. J., D. S. Zrnic, and D. S. Sirmans: Doppler Weather Radar, *Proc. IEEE*, vol. 67, no. 11, pp. 1522–1553, 1979.

11. Stimson, G. W.: "Introduction to Airborne Radar," Hughes Aircraft Company, El Segundo, Calif., 1983, pt. 7.

12. Hovanessian, S. A.: Medium PRF Performance Analysis, *IEEE Trans.*, vol. AES-18, pp. 286–296, May 1982.

13. Aronoff, E., and N. M. Greenblatt: Medium PRF Radar Design and Performance, *20th Tri-Service Radar Symp.*, 1974. Reprinted in Barton, D. K.: "CW and Doppler Radars," vol. 7, Artech House, Norwood, Mass., 1978, sec. IV-7, pp. 261–276.

14. Long, W. H., and K. A. Harriger: Medium PRF for the AN/APG-66 Radar, *Proc. IEEE*, vol. 73, pp. 301–311, February 1985.

15. Goetz, L. P., and J. D. Albright: Airborne Pulse Doppler Radar, *IRE Trans.*, vol. MIL-5, pp. 116–126, April 1961. Reprinted in Barton, D. K.: "CW and Doppler Radars," vol. 7, Artech House, Norwood, Mass., 1978, sec. IV-3, pp. 215–225.

16. Skolnik, M. I.: "Introduction to Radar Systems," 2d ed., McGraw-Hill Book Company, New York, 1984, chap. 4.

17. Finn, H. M., and R. S. Johnson: Adaptive Detection Mode with Threshold Control as a Function of Spatially Sampled Clutter-Level Estimates, *RCA Rev.*, pp. 414–464, September 1968.

18. Steenson, B. O.: Detection Performance of a Mean-Level Threshold, *IEEE Trans.*, vol. AES-4, pp. 529–534, July 1968.

19. Rohling, H.: Radar CFAR Thresholding in Clutter and Multiple Target Situations, *IEEE Trans.*, vol. AES-19, pp. 608–621, July 1983.

20. Hansen, V. G.: Constant False Alarm Rate Processing in Search Radars, *Proc. IEEE Int. Radar Conf.*, pp. 325–332, London, 1973.

21. Farrell, J., and R. Taylor: Doppler Radar Clutter, *IEEE Trans.*, vol. ANE-11, pp.

162–172, September 1964. Reprinted in Barton, D. K.: "CW and Doppler Radars," vol. 7, Artech House, Norwood, Mass., 1978, sec. VI-2, pp. 351–361.

22. Helgostam, L., and B. Ronnerstam: Ground Clutter Calculation for Airborne Doppler Radar, *IEEE Trans.*, vol. MIL-9, pp. 294–297, July–October 1965.

23. Friedlander, A. L., and L. J. Greenstein: A Generalized Clutter Computation Procedure for Airborne Pulse Doppler Radars, *IEEE Trans.*, vol. AES-6, pp. 51–61, January 1970. Reprinted in Barton, D. K.: "CW and Doppler Radars," vol. 7, Artech House, Norwood, Mass., 1978, sec. VI-3, pp. 363–374.

24. Ringel, M. B.: An Advanced Computer Calculation of Ground Clutter in an Airborne Pulse Doppler Radar, *NAECON '77 Rec.*, pp. 921–928. Reprinted in Barton, D. K.: "CW and Doppler Radars," vol. 7, Artech House, Norwood, Mass., 1978, sec. VI-4, pp. 375–382.

25. Jao, J. K., and W. B. Goggins: Efficient, Closed-Form Computation of Airborne Pulse Doppler Clutter, *Proc. IEEE Int. Radar Conf.*, pp. 17–22, Washington, 1985.

26. Harvey, D. H., and T. L. Wood: Designs for Sidelobe Blanking Systems, *Proc. IEEE Int. Radar Conf.*, pp. 410–416, Washington, 1980.

27. Maisel, L.: Performance of Sidelobe Blanking Systems, *IEEE Trans.*, vol. AES-4, pp. 174–180, March 1968.

28. Finn, H. M., R. S. Johnson, and P. Z. Peebles: Fluctuating Target Detection in Clutter Using Sidelobe Blanking Logic, *IEEE Trans.*, vol. AES-7, pp. 147–159, May 1971.

29. Mooney, D. H.: Post Detection STC in a Medium PRF Pulse Doppler Radar, U.S. Patent 690,754, May 27, 1976.

30. Skillman, W. A.: "SIGCLUT: Surface and Volumetric Clutter-to-Noise, Jammer and Target Signal-to-Noise Radar Calculation Software and User's Manual," Artech House, Norwood, Mass., 1987.

31. Ziemer, R. E., and J. A. Ziegler: MTI Improvement Factors for Weighted DFTs, *IEEE Trans.*, vol. AES-16, pp. 393–397, May 1980.

32. Skillman, W. A.: "Radar Calculations Using the TI-59 Programmable Calculator," Artech House, Norwood, Mass., 1983, p. 308.

33. Skillman, W. A.: "Radar Calculations Using Personal Computers," Artech House, Norwood, Mass., 1984.

34. Ward, H. R.: Doppler Processor Rejection of Ambiguous Clutter, *IEEE Trans.*, vol. AES-11, July 1975. Reprinted in Barton, D. K.: "CW and Doppler Radars," vol. 7, Artech House, Norwood, Mass., 1978, sec. IV-11, pp. 299–301.

35. Fletcher, R. H., Jr., and D. W. Burlage: An Initialization Technique for Improved MTI Performance in Phased Array Radar, *Proc. IEEE*, vol. 60, pp. 1551–1552, December 1972.

36. Skillman, W. A., and D. H. Mooney: Multiple High-PRF Ranging, *Proc. IRE Conf. Mil. Electron.*, pp. 37–40, 1961. Reprinted in Barton, D. K.: "CW and Doppler Radars," vol. 7, Artech House, Norwood, Mass., 1978, sec. IV-1, pp. 205–213.

37. Hovanessian, S. A.: An Algorithm for Calculation of Range in Multiple PRF Radar, *IEEE Trans.*, vol. AES-12, pp. 287–289, March 1976.

38. Ore, O.: "Number Theory and Its History," McGraw-Hill Book Company, New York, 1948, pp. 246–249.

39. Goetz, L. P., and W. A. Skillman: Master Oscillator Requirements for Coherent Radar Sets, *IEEE-NASA Symp. Short Term Frequency Stability*, NASA-SP-80, November 1964.

40. Raven, R. S.: Requirements for Master Oscillators for Coherent Radar, *Proc. IEEE*, vol. 54, pp. 237–243, February 1966. Reprinted in Barton, D. K.: "CW and Doppler Radars," vol. 7, Artech House, Norwood, Mass., 1978, sec. V-1, pp. 317–323.

41. Gray, M., F. Hutchinson, D. Ridgely, F. Fruge, and D. Cooke: Stability Measurement

Problems and Techniques for Operational Airborne Pulse Doppler Radar, *IEEE Trans.*, vol. AES-5, pp. 632–637, July 1969.

42. Acker, A. E.: Eliminating Transmitted Clutter in Doppler Radar Systems, *Microwave J.*, vol. 18, pp. 47–50, November 1975. Reprinted in Barton, D. K.: "CW and Doppler Radars," vol. 7, Artech House, Norwood, Mass., 1978, sec. V-3, pp. 331–336.

43. Black, H. S.: "Modulation Theory," D. Van Nostrand Company, Princeton, N.J., 1953, p. 265.

44. Barton, D. K.: "Radar Systems Analysis," Prentice-Hall, Englewood Cliffs, N.J., 1964, p. 206.

45. Ziemer, R. E., T. Lewis, and L. Guthrie: Degradation Analysis of Pulse Doppler Radars Due to Signal Processing, *NAECON 1977 Rec.*, pp. 938–945. Reprinted in Barton, D. K.: "CW and Doppler Radars," vol. 7, Artech House, Norwood, Mass., 1978, sec. IV-12, pp. 303–312.

46. Marcum, J. I.: A Statistical Theory of Target Detection by Pulsed Radar, *IRE Trans.*, vol. IT-6, pp. 59–267, April 1960.

47. Swerling, P.: Probability of Detection for Fluctuating Targets, *IRE Trans.*, vol. IT-6, pp. 269–308, April 1960.

48. Mooney, D., and G. Ralston: Performance in Clutter of Airborne Pulse MTI, CW Doppler and Pulse Doppler Radar, *IRE Conv. Rec.*, vol. 9, pt. 5, pp. 55–62, 1961. Reprinted in Barton, D. K.: "CW and Doppler Radars," vol. 7, Artech House, Norwood, Mass., 1978, sec. V1-1, pp. 343–350.

49. Ringel, M. B.: Detection Range Analysis of an Airborne Medium PRF Radar, *IEEE NAECON Rec.*, Dayton, Ohio, pp. 358–362, 1981.

50. Holbourn, P. E., and A. M. Kinghorn: Performance Analysis of Airborne Pulse Doppler Radar, *Proc. IEEE Int. Radar Conf.*, pp. 12–16, Washington, 1985.